Biomarker evidence for the depositional environment of basinal UK Mississippian mudstones

Michael James Edward Sims[1]*, Mark A. Sephton[1], Jonathan S. Watson[1], Alastair J. Fraser[1] and Christopher H. Vane[2]

[1]Department of Earth Science and Engineering, Imperial College London, South Kensington Campus, SW7 2AZ, UK

[2]British Geological Survey, Keyworth, Nottinghamshire NG12 5GG, UK

MJES, 0000-0002-1810-0339

*Correspondence: m.sims18@imperial.ac.uk

Abstract: The regional character of organic matter types and depositional conditions of Pendleian, Brigantian and Arnsbergian mudstones between the Craven Basin and the Widmerpool Gulf was compared through interpretation of biomarker and pyrolysis data from 201 samples recovered from nine boreholes. The Carboniferous seaways have been determined to commonly host dysoxic conditions, enabling the preservation of a mixture of marine and terrestrial organic matter types. Photic zone anoxia, established by the presence of aryl isoprenoids, was determined to be persistent during 'marine' conditions represented by marine band, high-sea-level and carbonate facies. The observation and correlation of diasteranes and trisnorneohopane/trisnorhopane ratios within the samples and to other maturity parameters highlighted a significant clay mineral catalytic and/or hydrocarbon retention effect in the samples. This influenced both biomarkers and programmed pyrolysis thermal maturity indices such as T_{max}, reducing the reliability of such results for interpreting the burial depth, and ultimately reserve potential.

Supplementary material: Tables of biomarker ratios and programmed pyrolysis data for each sample are available at https://doi.org/10.6084/m9.figshare.c.6988037

The Carboniferous geology of northern England provides a record of an ancient epicontinental seaway. The lithofacies recorded from the shelf, basin and deltas of the seaway has hosted hydrocarbon, metal and coal resource plays, which in turn has directed industrial endeavours as well as scientific enquiry across northern England (Waters *et al.* 2020*a*). Inspired by gas-in-place (GIP) estimates of 822–2281 TCF (Andrews 2013), the most recent industrial interest was focused on sources of unconventional gas from shale. The target source rocks were the Bowland Shale and Hodder Mudstone formations. Understanding the controls on organic matter type and its distribution in the prospective rocks has been identified as a key characteristic to determine the potential of unconventional resources (Andrews 2013). Different studies have identified differing controls on the organic matter type. Using programmed pyrolysis data, mixed Type II/III kerogens have been inferred from comparison of S2 and total organic carbon (TOC) content (Gross *et al.* 2015; Waters *et al.* 2020*b*). However, studies on kerogen kinetics and palynology have attested to Type II and I kerogen generative capability (Yang *et al.* 2016; Hennissen *et al.* 2017; Newport *et al.* 2020). Environmental factors controlling water column stratification, redoxclines and sediment source have been cited as generating variability in the potential of the formations by preferentially preserving organic matter (Gross *et al.* 2015; Emmings *et al.* 2020*a*); understanding these is vital to determine the Mississippian basinal setting and resources sourced.

The main unconventional target in the Carboniferous succession of northern England is the Bowland Shale Formation, defined as a grouping of the regional formations of the Holywell, Edale and Bowland Shale formations (Waters *et al.* 2009). The formation is described as dark-grey fissile to blocky hemipelagic mudstones, which transitioned with decreasing age from a calcareous to siliciclastic mineralogy (Waters *et al.* 2009, 2020*b*; Clarke *et al.* 2018). Other relevant formations include the Morridge formations, which have been used as analogue studies or alternative targets, despite these formations having a greater siliciclastic content (i.e. Könitzer *et al.* 2014; Gross *et al.* 2015; Słowakiewicz *et al.* 2015; Yang *et al.* 2016; Hennissen *et al.* 2017; Whitelaw *et al.* 2019). Data from microscale sealed vessel (MSSV) pyrolysis on the source rock demonstrated a promising Type II kerogen productive capability (Yang *et al.* 2016). Recent resource

From: Emmings, J. F., Parnell, J., Stephenson, M. H. and Lodhia, B. H. (eds) 2024. *The Bowland Shale Formation, UK: Processes and Resources*. Geological Society, London, Special Publications, **534**, 123–146.
First published online March 22, 2024, https://doi.org/10.1144/SP534-2022-225

estimates derived from high-pressure water pyrolysis on Arnsbergian and Pendleian samples have reduced the GIP estimates to 140 ± 55 TCF, further limited by a 10% economic recovery for northern England (Whitelaw *et al.* 2019). The source rock facies were confined primarily within half-graben basins; however, deposition extended onto the shelves in association with maximum flooding surfaces (Waters *et al.* 2020*b*). This was calculated to have occurred in a 110 ka cycle for flooding surfaces with closely related faunal assemblages, and a 400 ka cycle is typically associated with more significant faunal change (Waters and Condon 2012). The combined influence of sea-level fluctuation with proximity to delta systems generated lateral and stratigraphic heterogeneity in the preserved organic fraction (Gross *et al.* 2015; Emmings *et al.* 2020*b*).

Emmings *et al.* (2020*a*) determined that the chemistry of the Pendleian water column in the Craven Basin had an oscillating palaeoredox zone that maintained euxinic conditions during transgressive-highstand sea-level states, becoming more oxidized with falling or low sea-level states. Similarly, Arnsbergian mudstones from the distal Widmerpool Gulf were deposited under anoxic conditions that extended to the photic zone during high sea levels, with low sea-level associated turbidite sediments associated with increased volumes of terrestrial organic matter, reduced salinity and more dysoxic to oxic conditions prevailing in the water column (Gross *et al.* 2015).

Oxic or aerobic water is classified as containing over 2 ml l^{-1} of oxygen, representing well-ventilated water inducing no biological stress on fauna and enabling degradation of dispersed organic matter in sediment (Algeo and Li 2020). Anoxia represents the total lack of dissolved oxygen, conditions that are often associated with the biological use of sulfate in oxidation–reduction reactions (Algeo and Li 2020). Anoxic conditions are ferruginous if dissolved Fe^{2+} is present, or euxinic if H_2S is present instead (Algeo and Li 2020). Dysoxia is a commonly applied term in geoscience that relates to the impact of reduced oxygen levels (2–0.5 ml l^{-1}) to fauna distribution and diversity and organic enrichment (Tyson and Pearson 1991). Sub-oxic is used to describe water with very low (0.7–0 ml l^{-1}) oxygen concentrations, where the depositional environments lack significant bioturbation and macro-fossils (Breck 1974; Tyson and Pearson 1991) and reduction reactions involving nitrate, manganese or iron are facilitated by microbial organisms.

Biomarkers represent the biomolecular record of organisms existing within the depositional regime in which sedimentary rocks are deposited. Some biomarkers such as pristane/phytane (Pr/Ph) may be interpreted as indicative of palaeoredox conditions (Didyk *et al.* 1978). Published values for Pr/Ph ratios are shown in Figure 1 where oxic waters are represented by values over 3, dysoxic–sub-oxic as values between 2 and 0.8, while anoxic to euxinic values will be lower than 0.8. Other biomarkers such as aryl isoprenoids have been proven to represent the presence of water column euxinia that extends to the photic zone (Schwark and Frimmel 2004; Gross *et al.* 2015). The change of aryl isoprenoids has also been included in Figure 1. High levels of C_{35} homohopanes have also been related to the presence of anoxia, as the hopanes are more likely to have originated from bacterial groups. Ts/Tm as a biomarker index may also demonstrate Eh effects at the sediment–water interface if it is anoxic (Peters *et al.* 2005).

In the current study, 201 samples from the Central Pennines and Craven Basin were analysed to develop a spatially distributed dataset on biomarker environmental indices, representing the first study to analyse organic geochemical trends across multiple boreholes dated from the Brigantian to the Arnsbergian–Chokierian boundary. To relate the study to other regional works, programmed pyrolysis was undertaken on all samples to understand the bulk geochemical source rock character of Mississippian mudstones. Biomarker results were produced from extractable organic matter (EOM) to delineate changes pertaining to salinity, water column anoxia and the provenance of organic matter across the basins.

Geological setting

The Carboniferous basins of northern England began rifting in the Devonian, relating to collapse of the Caledonian Orogen following the closure of the Iapetus Suture (Fraser and Gawthorpe 2003). The Late Devonian–Carboniferous subduction of the Rheno-Hercynian oceanic crust contributed to additional thermal and magmatic input, generating crustal stretching and Dinantian rift basin formation (Leeder 1988; Timmerman 2004). Far-field orogenic influences contributed transtensional forces enabling periodic eastward extension through which compression is accommodated via 'crustal escape' or extrusion mechanisms (Maynard *et al.* 1997; Fraser and Gawthorpe 2003).

Rifting initiated over continental conditions, with subsidence enabling the formation of lacustrine and transgressive horizons within the Devonian sequences. By the Early Carboniferous, marine to periodically sub-aerial conditions were established, depositing the Carboniferous Limestone Supergroup of Waters *et al.* (2009). The earliest stratigraphy was dominated by regional shallow-water carbonates. This depositional environment persisted on the shelves while the basins rifted, forming ramp and

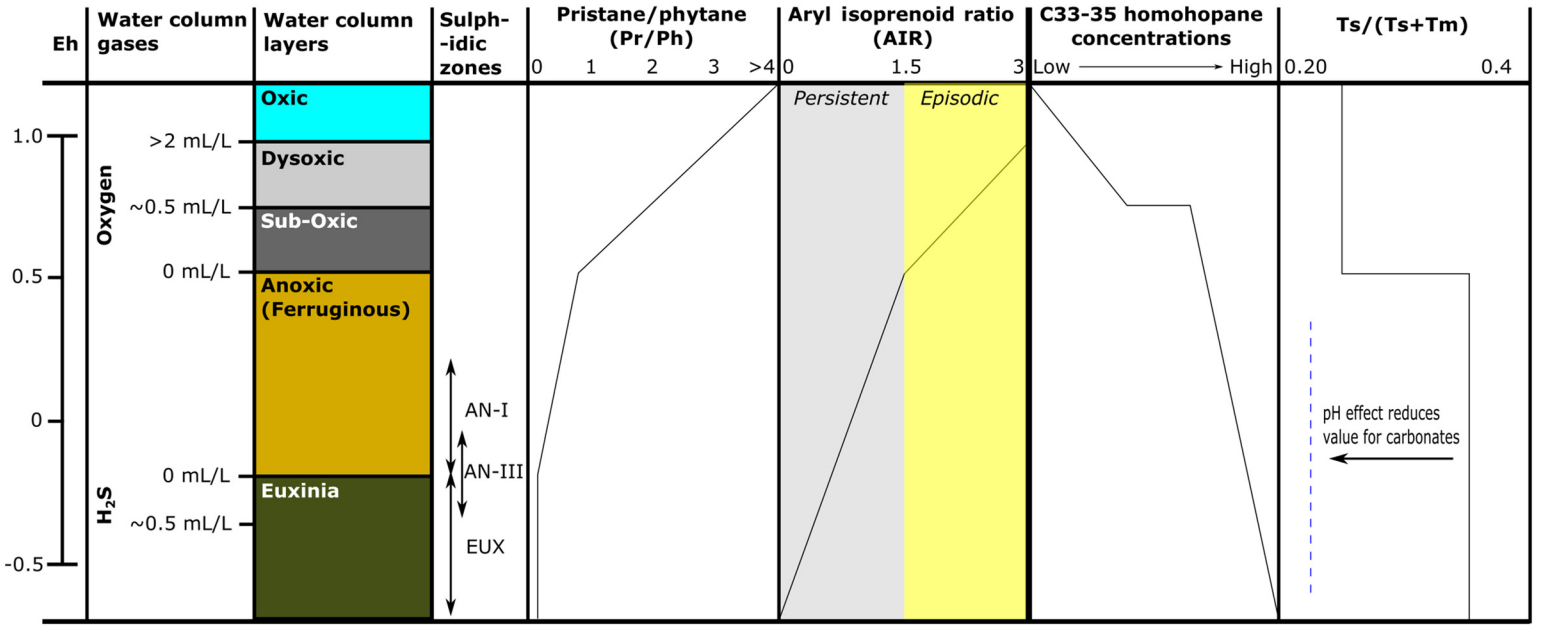

Fig. 1. Oxic–anoxic levels as defined by Tyson and Pearson (1991) against Eh values and oxygen and H_2S concentrations (Algeo and Li 2020). The sulfidic zones identified by Emmings *et al.* (2020*a*) have been included for reference to relate observations from trace-element composition with organic biomarkers. Ratios of palaeoredox indicative biomarkers have been included after Peters *et al.* (2005) demonstrating expected levels for each of the zones.

slope architectures into the depocentres (Riley 1990; Fraser and Gawthorpe 2003). The margins would periodically collapse into the depocentres forming a framework of calciturbidites and other transport deposits interbedded with calcareous mudstones.

The Bowland Shale Formation and its diachronous counterparts were deposited under late synrift and early post-rift conditions, onlapping the carbonate margin sediments (Waters *et al.* 2020*b*). The source rock interval was confined to the basin depocentres during the Dinantian, but 'drowning' of palaeohighs enabled draping of the source rock onto the carbonate highs (Kirby *et al.* 2000; Waters *et al.* 2020*b*). Palaeowater depths of depocentres were interpreted to be >300 m by Fraser and Gawthorpe (2003).

Siliciclastic turbidites acted as precursors to basin infill by the deltaic Millstone Grit Group (Waters *et al.* 2020*b*). Infill of the basins occurred in a stepwise staged process as carbonate highs provided a barrier directing sedimentation through erosional valley systems (Fraser and Gawthorpe 2003; Waters *et al.* 2020*b*), generating diachroneity in the age at the top of the Bowland Shale. Within the Millstone Grit Group, periods of deltaic influence were broken by the deposition of organic-rich mudstones such as the Caton Shales (Clarke *et al.* 2018), extending source rock deposition into at least the late Arnsbergian (Waters *et al.* 2020*b*). Within the Widmerpool Gulf, Arnsbergian-age sediments are represented by the Morridge Formation, which includes distal turbidites and hemipelagic mudstones (Waters *et al.* 2009). Brigantian to Pendleian mudstones from the Craven Basin contain a relatively high detrital mineral fraction and an associated mixed Type II/III organic matter composition, particularly in the Upper Bowland Shale (Clarke *et al.* 2018). Palynological interpretation of their Widmerpool Gulf counterparts revealed a plethora of microbially degraded organic matter types and evidence of algal groups such as *Botryococcus* spp. (Könitzer *et al.* 2016; Hennissen *et al.* 2017; Hennissen and Montesi 2020).

Experimental methods

Core logging, sampling and preparation

Boreholes held at the National Geological Repository core store in Keyworth were studied during the project. Cores were selected based on whether they contained representative samples of Carboniferous mudstones. The cores were required to have been tied to the goniatite biostratigraphy of the UK Carboniferous, through either core logs available via the BGS GeoIndex, industry reports available through the UK Onshore Geophysical Library (UKOGL), academic papers or PhD theses. Core chips were taken where possible at regular intervals through the cores.

Core chips were washed with *n*-pentane to remove any surface labile hydrocarbons and contaminants. The samples were powdered using a ceramic mortar and pestle to an approximate size of <30 μm. A single powdered aliquot for the current study was produced, weighing *c.* 3–5 g. This was split as required for Rock-Eval 6, and solvent extraction ahead of biomarker analysis.

Rock-Eval 6 programmed pyrolysis

Programmed pyrolysis is a commercially available standard methodology for studying source rock quality and richness through the measurement of produced volatile products such as hydrocarbons, CO_2 and CO, from the staged heating of sample material (Espitalié *et al.* 1977; Lafargue *et al.* 1998). The measurements of pyrolytically released volatiles are often compared to determine the kerogen types and whether the rock is prone to producing gas or oil (Jarvie 2012; Peters *et al.* 2015). Furthermore, the temperature at which maximum hydrocarbon generation occurs (T_{max}) is known to relate to the maturity of samples as an alternative to vitrinite reflectance (Espitalié 1986). The use of the method formed a central focus of many Bowland Shale specific studies (i.e. Gross *et al.* 2015; Hennissen *et al.* 2017; Newport *et al.* 2020; Waters *et al.* 2020*b*); thus the analysis from this project provides a direct comparison to other regional studies. This project made use of the Rock-Eval 6 pyrolysis and oxidation capabilities hosted at the British Geological Survey to standardize and compare measurements with published results such as Waters *et al.* (2020*b*).

Powdered aliquots of samples were analysed using a Rock-Eval 6 analyser configured in standard mode, pyrolysis and oxidation as a serial process (as in Waters *et al.* 2020*b*). Powdered rock samples were heated isothermally and maintained for 3 minutes at 300°C to release free hydrocarbons. Subsequently, a heating ramp of 25°C per minute was used to increase the temperature from 300 to 650°C, cracking non-volatile organic matter in an inert atmosphere of N_2. Hydrocarbons released from this process were measured using a flame ionizing detector (FID), and CO with CO_2 were measured using an infrared (IR) cell. From the pyrogram FID and IR peaks, the S1, S2 and S3 parameters were given and used to calculate hydrogen index (HI), oxygen index (OI) and production index (PI) as per the equations in Lafargue *et al.* (1998). After pyrolysis, the samples were oxidized from 300 to 850°C to determine the residual carbon in the rock, which was used with data from the S2 and S3 peaks to derive the TOC content.

Gas chromatography mass spectrometry

Around 1 to 1.5 g of powdered aliquot were added to clean test tubes, with 10 µl of a prepared internal standard of squalane and *p*-terphenyl; 4 ml of dichloromethane (DCM)/methanol 93:7 v/v were added to the samples, which were subjected to 5 minutes of sonication and centrifuged for 3 minutes at 1.5 rpm. The resultant supernatant was transferred into a new test tube and the process repeated four times per sample. Copper turnings were added to the supernatant and the volume was reduced and replaced with DCM:*n*-hexane 1:1 v/v mixture before the aliphatic and aromatic fractions were eluted using DCM:*n*-hexane 1:1 v/v by column chromatography using activated alumina powder. The fraction was further concentrated to 0.5 ml.

Analysis was conducted using an Agilent Technologies 7890A gas chromatography (GC) system coupled to a 5975C mass spectrometer (MS). The GC injector was run in a splitless mode (1 µl) with the column flow rate set at 1.1 ml min^{-1}. A J&W scientific DB-5MS capillary column was used for compound separation and helium employed as a carrier gas. The GC oven was started at 40°C for 2 minutes; this was raised at a rate of 5°C min^{-1} to 310°C and held for 14 minutes. Mass spectra were acquired in electron impact mode in the scan range of 50–500 a.m.u. The data was qualitatively and quantitatively studied using the Mass Hunter workstation software package (Agilent Technologies Inc. 2016). Biomarkers were identified and indices were determined by comparative investigation of peak areas for each chromatograph produced. A list of identified biomarkers is provided in Table 1.

X-ray diffraction

X-ray diffraction (XRD) analysis was completed using a PANalytical X'Pert Pro Alpha-1 system hosted at the Natural History Museum, London. The unit was set up with a cobalt source tube that recorded a diffraction angle range from 4° to 90°. For each analysis, 1 g of powdered sample material was backloaded into metal holders. Mineral peaks were picked using the XPERT Highscore Plus software package (Degen *et al.* 2014), and samples were quantified utilizing Profex open source (Döbelin and Kleeberg 2015) XRD Rietveld refinement software.

Samples and stratigraphic correlation

The 201 samples included in the current study were taken between nine boreholes in northern England, either at equivalent ages or a range of depths to determine variation in biomarker trends temporally and spatially. The distribution of cores v. time is illustrated in Figures 2 and 3. From core material dated to the Arnsbergian or younger, 141 samples were taken, mostly focusing on the Carsington Dam Reconstruction-C4 ($n = 53$) and the Wray boreholes ($n = 47$). The Pendleian to Brigantian had a total of 60 samples taken between four boreholes. The distributions of samples are shown in Figures 2a and 3a showing well locations, and Figures 2b and 3b demonstrating sampling locations against sedimentary logs.

In the Wray geothermal borehole, the E_{2b} marine band is marked by the identification of *Cravenoceras subplicatum* at *c.* 120.45 m (Brandon *et al.* 1998). Beneath the E_{2b} marine band, the Wards Sandstone representing a delta top would have eroded any coeval representation of the $E_{2a}3$ *Eumorphoceras yatesae* marine band. The underlying siltstone facies represent the Close Hill Siltstone and may contain the $E_{2a}2b$ marine band of Brandon *et al.* (1995). This borehole represents Arnsbergian strata in the Craven Basin, allowing correlation with datasets from the Widmerpool Gulf equivalents.

The Croft House borehole sited upon the Askrigg Block encountered similar strata to the Wray geothermal borehole. The E_{2b} marine band is attributed to 40–42 m depth as in Brandon *et al.* (1995). This is positioned above the Red Scar Grit and E_{2a} equivalent shales that relate to the Wards Sandstone and Close Hill Siltstones of the Wray geothermal borehole.

In the Carsington Dam Reconstruction-C4 borehole, the E_{2b} marine band is recognized through the presence of *Cravenoceratoides edalensis* from 22.52 m, with cravenoceratid fragments first appearing from 26.67 m. The $E_{2a}3$ marine band is present in this borehole and was logged by Könitzer *et al.* (2014) from *c.* 27.9 to 33.85 m. Both the $E_{2a}2a$ and $E_{2a}2b$ marine bands were first correlated between the Carsington Dam locality, the Duffield borehole and the Bowland basin by Brandon *et al.* (1995); Könitzer *et al.* (2014) logged an unidentified $E_{2a}2$ marine band from 52.6 to 53.1 m in the borehole. Based on published logs this is likely to be the $E_{2a}2b$ marine band (Brandon *et al.* 1995). At the Carsington locality, the borehole records no delta top sandstone and represents a distal setting with consistent marine conditions influenced by siliciclastic turbidites (Könitzer *et al.* 2014). Rempstone-1 was also logged and studied, which represents E_2 mudstones in a turbiditic setting.

The logged section of the Ipstones Edge borehole contains the *Isohomoceras subglobosum* $H_{1a}1$ and the $E_{2c}2$–4 *Nuculoceras nuculum* marine bands (Chisholm *et al.* 1988; Morton *et al.* 2015). The lower section of the borehole is divided by the Hurdlow Sandstones, which are described as a turbiditic unit found in the Goyt Trough and western Widmerpool Gulf (Morton *et al.* 2015). The Hurdlow

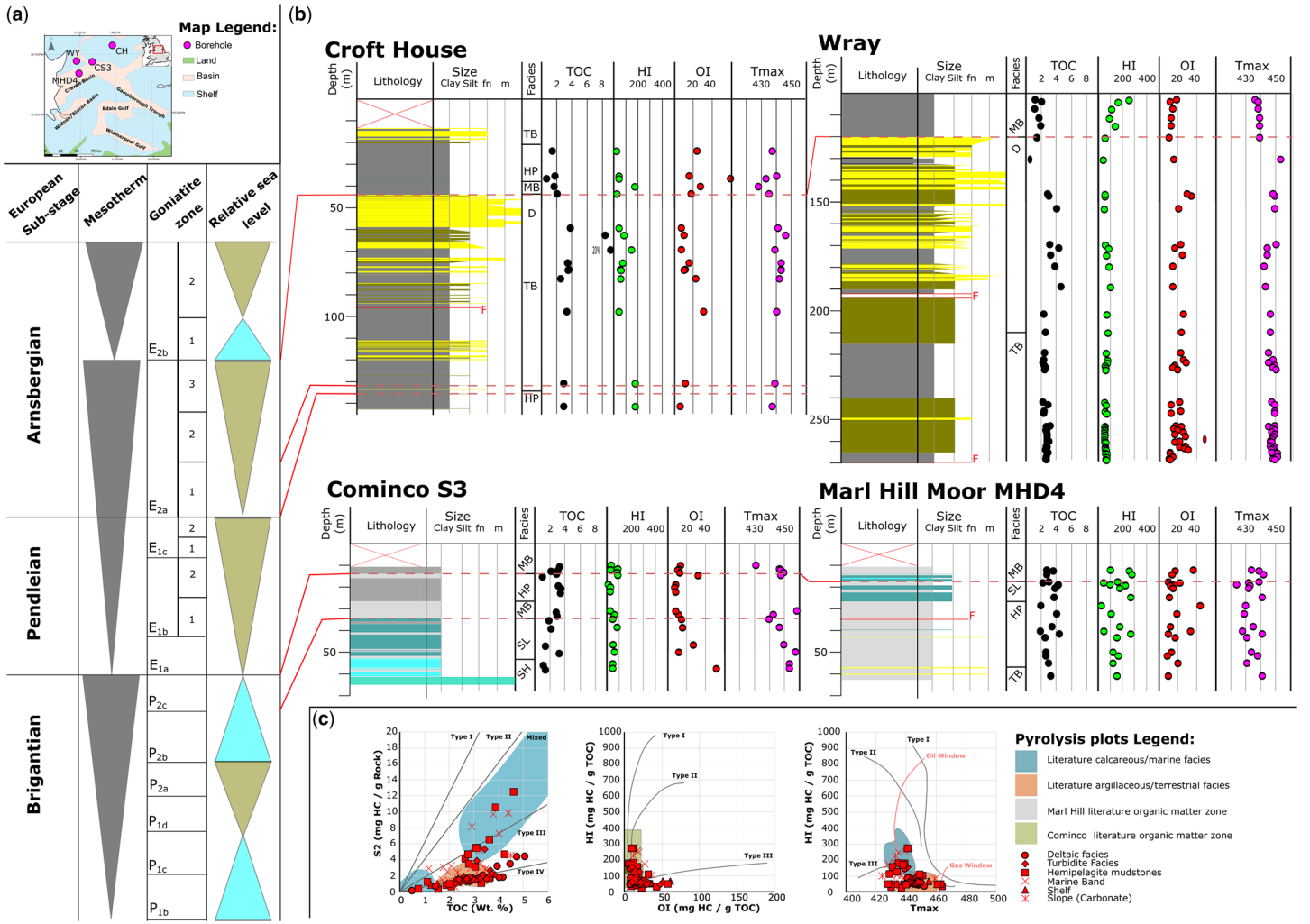
(a)
Map Legend:
Borehole
Land
Basin
Shelf
WY
CH
CS3
MHD4
Cleveland Basin
Widmerpool Gulf
Edale Gulf
Gainsborough Trough
European Sub-stage
Mesotherm
Goniatite zone
Relative sea level
Arnsbergian
Pendleian
Brigantian
E2b
E2a
E1c
E1b
E1a
P2c
P2b
P2a
P1d
P1c
P1b
(b)
Croft House
Wray
Cominco S3
Marl Hill Moor MHD4
Depth (m)
Lithology
Size
Clay Silt fn m
Facies
TOC
HI
OI
Tmax
TB
HP
MB
D
SL
SH
(c)
S2 (mg HC / g Rock)
TOC (Wt. %)
Type I
Type II
Mixed
Type III
Type IV
HI (mg HC / g TOC)
OI (mg HC / g TOC)
Tmax
Oil Window
Gas Window
Pyrolysis plots Legend:
Literature calcareous/marine facies
Literature argillaceous/terrestrial facies
Marl Hill literature organic matter zone
Cominco literature organic matter zone
Deltaic facies
Turbidite Facies
Hemipelagite mudstones
Marine Band
Shelf
Slope (Carbonate)

Sandstones overlie an undated mudstone, which is tentatively assigned to the $E_{2b}3$ zone.

Waters *et al.* (2020*b*) highlighted that, in the Widmerpool Gulf, only samples below the $E_{1b}2$ *Tumulites pseudobilinguis* marine band can be considered as being representative of the Bowland Shale Formation and that strata younger than that horizon should be considered as representative of the Morridge Formation. To test similarities of conditions within the Widmerpool Gulf, the Lees Farm borehole was studied. From borehole reports, the Lees Farm borehole has the E_{1a} marine band sited at 12.7 m depth, recognized by *Emstites leion* at 11.18 m depth. Below this at 23.30 m depth, *Neoglyphioceras* sp. represents P_2 zone Brigantian age strata diachronous with the Lower Bowland Shale. The Wardlow Mires boreholes were sited on the Derbyshire High, recording strata from the E_{2a} *Eumorphoceras bisulcatum* zone to the P_2 zones represented by *Neoglyphioceras* sp. and *Sudeticeras* sp.

The Marl Hill-4 borehole has been extensively studied, and the biostratigraphic positioning is based on the resulting publications (see Emmings *et al.* 2019, 2020*a*, *b*). This puts the *E. leion* E_{1a} zone at *c.* 17 m depth, marking the boundary of the Upper and Lower Bowland Shale as they appear in the Craven Basin. Cominco-S3 provides an equivalent representation of this boundary at 13.72 m depth for comparison. At 31.50 m depth in the Cominco-S3 borehole, the P_{2b} to P_{2c} boundary was interpreted based on the upper observation of *Neoglyphioceras* sp. representing the Middle Brigantian.

Results

TOC content and programmed pyrolysis

The whole dataset of samples has a mean average TOC content of 3.14%, which ranges from 0.42% in the Croft House borehole to 20.16% in the Wardlow Mires core. Splitting the sample set into regions gives an average TOC content of 3.08% in the Craven Basin and 3.20% in the Central Pennines. In terms of the cores sampled in the Craven Basin, Cominco-S3 had the lowest average at 2.63% and Croft House had the highest average TOC at 4.37%. Comparatively, in the East Midlands, Ipstones Edge had the lowest of sampled wells at 1.80%, while Rempstone-1 had the highest mean TOC content of 5.74%. Figures 2 and 3 show TOC contents for the different boreholes; comparatively, the values show an overall greater abundance of TOC in the Widmerpool Gulf in comparison to the Craven Basin.

The S2 results from the total data give an average value of 5.52 mgHC g^{-1} rock. In the Craven Basin, the average value decreases to 2.92 mgHC g^{-1} rock, ranging from 1.70 mgHC g^{-1} rock in the Wray borehole to a high average of 5.61 mgHC g^{-1} rock in Marl Hill-MHD4. In the Central Pennines, the mean S2 is 7.60 mgHC g^{-1} rock, ranging from 1.86 mgHC g^{-1} in the Ipstones Edge borehole to 25.53 mgHC g^{-1} rock in Rempstone-1.

T_{max} results vary across the sample set between 421°C in the Ipstones Edge borehole and 464°C in the Cominco-S3 borehole. The mean value across all samples is 438°C. T_{max} was found to vary significantly within boreholes; for example, the Wardlow Mires core has a minimum T_{max} of 427°C at 8.71 m measured depth (MD) to 452°C at 105 m MD (Fig. 3b). Such a variation in T_{max} results is assumed to be incorrect for a standard geothermal gradient, which is attributed to lower S2 values associated with turbiditic and deltaic samples as in Figures 2b, c and 3b, c.

An average HI value of 144 mgHC g^{-1} TOC was calculated for the dataset (Figs 2c & 3c), split between a mean of 196 mgHC g^{-1} TOC in the East Midlands samples and 88 mgHC g^{-1} TOC in Lancashire–Yorkshire. The Wray borehole had the lowest HI at 66 mgHC g^{-1} TOC (Fig. 2b), while Rempstone-1 had the highest mean at 403 mgHC g^{-1} TOC (Fig. 3b). Plotting HI against T_{max} (Figs 2c & 3c) to determine maturity and kerogen type demonstrates a distribution of data points in the immature to mid oil window, varying between Type II and III kerogen classifications. From the S3 data, OI was calculated for all samples with a mean value of 19. Within the dataset ten samples have OI values over 40 mgCO_2 g^{-1} TOC.

Fig. 2. (**a**) Map of the location of northern England boreholes in relation to the structural basin framework of the Carboniferous seaways of northern England. Basins of northern England mapped after Fraser and Gawthorpe (1990), updated after Andrews (2013) and Lodhia *et al.* (2023). Well names are shortened as follows CH, Croft House; CS3, Cominco-S3; MHD4, Marl Hill Moor-MHD4; WY, Wray. (**b**) Core panels from Croft House, Wray, Cominco-S3 and Marl Hill Moor-MHD4. The TOC content is reported as wt%, HI is reported in mgHC g^{-1} TOC, OI in mgCO_2 g^{-1} TOC and T_{max} in °C. Cores have been positioned stratigraphically; solid red and dashed pink lines refer to identified biostratigraphic zonation as described in the text. Relative sea-levels interpreted from Waters and Condon (2012). The lithological key is the same as for Figure 3. (**c**) Common plots for interpreting organic matter type and maturity from programmed pyrolysis datasets. Zones describing calcareous and marine facies are from Newport *et al.* (2018) and Emmings *et al.* (2020*b*), showing that the majority of samples analysed align with published trends, particularly for argillaceous facies.

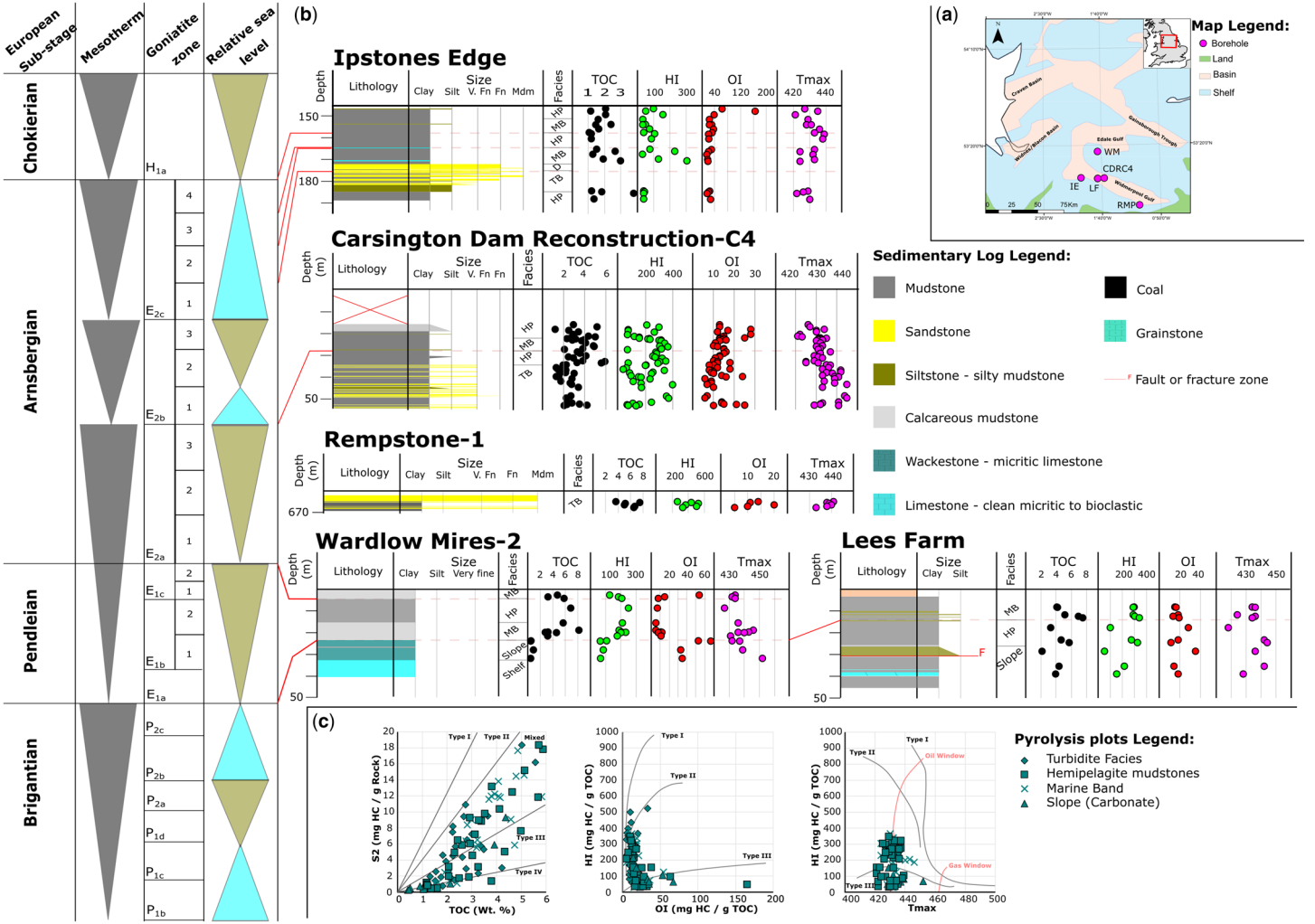
European Sub-stage
Mesotherm
Goniatite zone
Relative sea level
Chokierian
Arnsbergian
Pendleian
Brigantian
H1a
E2c
E2b
E2a
E1c
E1b
E1a
P2c
P2b
P2a
P1d
P1c
P1b
(b)
Ipstones Edge
Carsington Dam Reconstruction-C4
Rempstone-1
Wardlow Mires-2
Lees Farm
Depth
Lithology
Size
Facies
TOC
HI
OI
Tmax
(a)
Map Legend:
Borehole
Land
Basin
Shelf
WM
CDRC4
IE
LF
RMP
Sedimentary Log Legend:
Mudstone
Coal
Sandstone
Grainstone
Siltstone - silty mudstone
Fault or fracture zone
Calcareous mudstone
Wackestone - micritic limestone
Limestone - clean micritic to bioclastic
(c)
S2 (mg HC / g Rock)
TOC (Wt. %)
HI (mg HC / g TOC)
OI (mg HC / g TOC)
Tmax
Type I
Type II
Type III
Type IV
Mixed
Oil Window
Gas Window
Pyrolysis plots Legend:
Turbidite Facies
Hemipelagite mudstones
Marine Band
Slope (Carbonate)

Acyclic isoprenoids and n-alkanes

Both pristane and phytane were detected in all samples; the ratio of these ranged from 0.62 to 6.92 with a mean value around 1.55, which correlates with values previously published from the Craven Basin (Emmings *et al.* 2020*a*). Most samples were distributed within values of 0.8–1.8 (Figs 4b & 5b). Comparing the isoprenoids in Figures 4a and 5a to their *n*-alkane counterparts *n*-C_{17} and *n*-C_{18}, most samples have a ratio of less than 1. Samples mostly from the boreholes Croft House and Ipstones Edge plot above 1, alongside many of the Lees Farm borehole samples. The majority of samples fall into a mixed organic matter type and a mixed oxidizing–reduced setting according to those ratios.

The aliphatic content of the samples' EOM contained a suite of *n*-alkanes from *n*-C_{11} to *n*-C_{35}, although the higher abundances generally ranged from *n*-C_{13} to *n*-C_{33}. The percentile distribution of *n*-alkanes is orientated towards $C_{11–20}$, with $C_{21–25}$ representing the second highest distribution. This is reflected in calculated carbon distributions such as the terrigenous to aquatic ratio (TAR) in which most data points range below a ratio of 1 (Figs 4b & 5b). Carbon preference index (CPI) results range within the boreholes as shown in Figure 4b but modally plot close to a value of 1 for the Brigantian–Pendleian samples and are slightly elevated for Arnsbergian sample material (Fig. 5b), indicating a slight odd preference consistent with additional terrigenous organic matter.

Hopanes, terpanes and other 191 mass chromatogram peaks

The 191 terpane chromatogram is dominated by hopanes. Tricyclic and tetracyclic terpanes are also present, as shown in Figure 6, but were not quantified. 17α-trisnorhopane (Tm) and 18α-trisnorneohopane (Ts) were detected in all samples with a slight preference towards Tm in the peak heights. On average the C_{30} 17α-21β-hopane homologue has preference over C_{29}αβ, while the $C_{31–35}$ homohopane series has a stepwise downward trend through the homologues from C_{31} to C_{35}. This produced an average C_{35} homohopane index of 7% rising to a maximum of 16% in the Carsington Dam Reconstruction-C4 borehole and a minimum of 4% in the Wray borehole. Comparing hopane homologue ratios shows a mean $C_{31}R/C_{30}$ of 0.30, a mean C_{35}/C_{34} of ratio of 0.31 and for C_{29}/C_{30}, 0.77. Hopane isomerism shows a preference in the chromatograms towards the S isomer; this is reflected in the $22S/(22S + 22R)$ indices, which average 0.59 for C_{31}, 0.57 for C_{32} and 0.54 for C_{33}. C_{35} hopane isomerism averages significantly lower than the other indices owing to low concentrations and thus is not interpreted further. C_{34} isomerism is higher, averaging 0.64 for the whole sample set.

Rearranged hopanes were also observed in trace quantities. The C_{29} 18α(H)-30-norneohopane (C_{29}Ts) coeluted with C_{29} 17α-21β-hopane and was quantified by the area of the peak shoulder effect produced. The C_{30} 18α(H)-30-neohopane (C_{30}Ts) was identified by its relative retention indices to the C_{29}Ts shoulder and C_{30}αβ hopane. C_{30} and C_{29} 17α-diahopanes were widely observed. Trace doublet peaks between the C_{32}–C_{35} homohopane doublets (Fig. 6) may represent the presence of a diahopane homologue series. Additionally, a small peak representing a trace amount of C_{28} 28-norhopane was commonly observed eluting between C_{29} diahopane and C_{29}αβ/Ts; it was confirmed through a m/z 355 extracted ion chromatogram (EIC).

In addition to the hopane series, gammacerane was also widely detected, with a relatively small peak area (Fig. 6) in the samples analysed. The gammacerane index (GI) was calculated as $10 \times$ gammacerane/(gammacerane + C_{30} hopane). The average value for the sample set is *c.* 1. The range of values includes a maximum of 2.68 and minimum of 0.34; both values were recorded from the Carsington Dam Reconstruction-C4 borehole, but most samples across the entire set distribute between 0.5 and 1.5 GI. GI varies stratigraphically; enhanced levels occur around marine bands found in Cominco-S3, Marl Hill-4, Ipstones Edge and Carsington Dam Reconstruction-C4.

Steranes

The most common steranes in the EOM analysed were the C_{27}–C_{29} sterane homologues (Fig. 7). Of the steranes quantified there was a preference in the

Fig. 3. (**a**) Map of the location of sampled boreholes from the Central Pennines or East Midlands. The majority of samples were taken from within the Widmerpool Gulf Basin. Basins of northern England are included for reference as in Figure 2. Boreholes abbreviated as follows: WM, Wardlow Mires-2; CDRC4, Carsington Dam Reconstruction-C4; IE, Ipstones Edge; LF, Lees Farm; RMP, Rempstone-1. (**b**) Core panels from the aforementioned boreholes positioned stratigraphically. The TOC content is reported as wt%, HI is reported in mgHC g^{-1} TOC, OI in mgCO_2 g^{-1} TOC and T_{max} in °C. Solid red and dashed pink lines refer to identified biostratigraphic zonation as described in the text. Relative sea-levels interpreted from Waters and Condon (2012). (**c**) Plots for interpreting organic matter type and maturity from programmed pyrolysis datasets showing the range within the Central Pennine Dataset. The overall hydrocarbon generation potential interpreted from these plots is greater for this region.

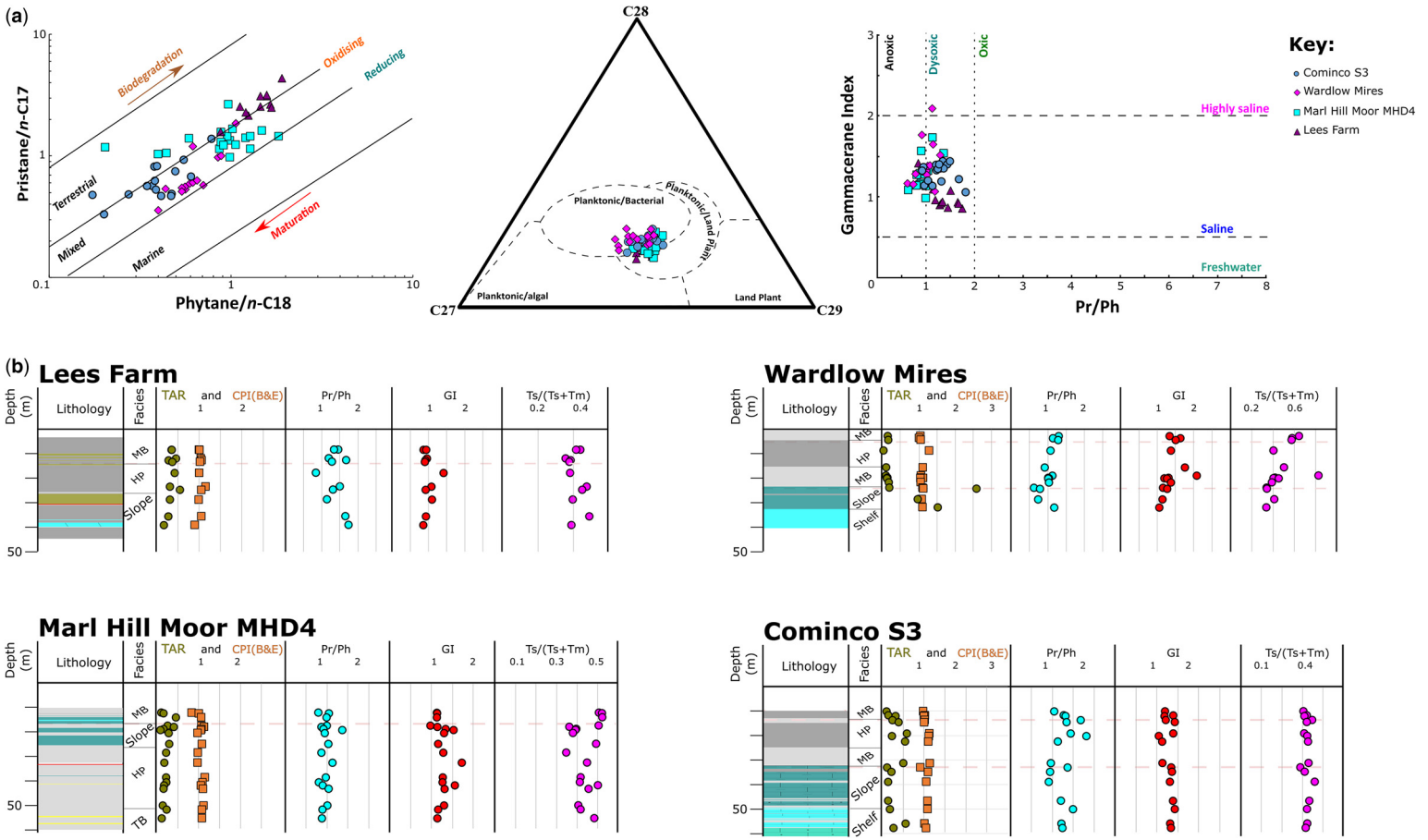

Fig. 4. (**a**) Biplots of biomarker indices (from left to right): pristane/*n*-C_{17} over phytane/*n*-C_{18} with organic matter type and depositional lines overlain, showing predominantly mixed kerogen type; ternary plot of sterane abundances based on the peak areas of the $C_{27–29}$ ααα*R* steranes; plot of gammacerane index (GI) over Pr/Ph. The majority of data points cluster in the saline dysoxic zone. (**b**) Biomarker log plots for Pendleian–Brigantian aged samples from across northern England showing relative trends in biomarker ratios. Carbon preference index (CPI) is interpreted after the Bray and Evans (1961) method.

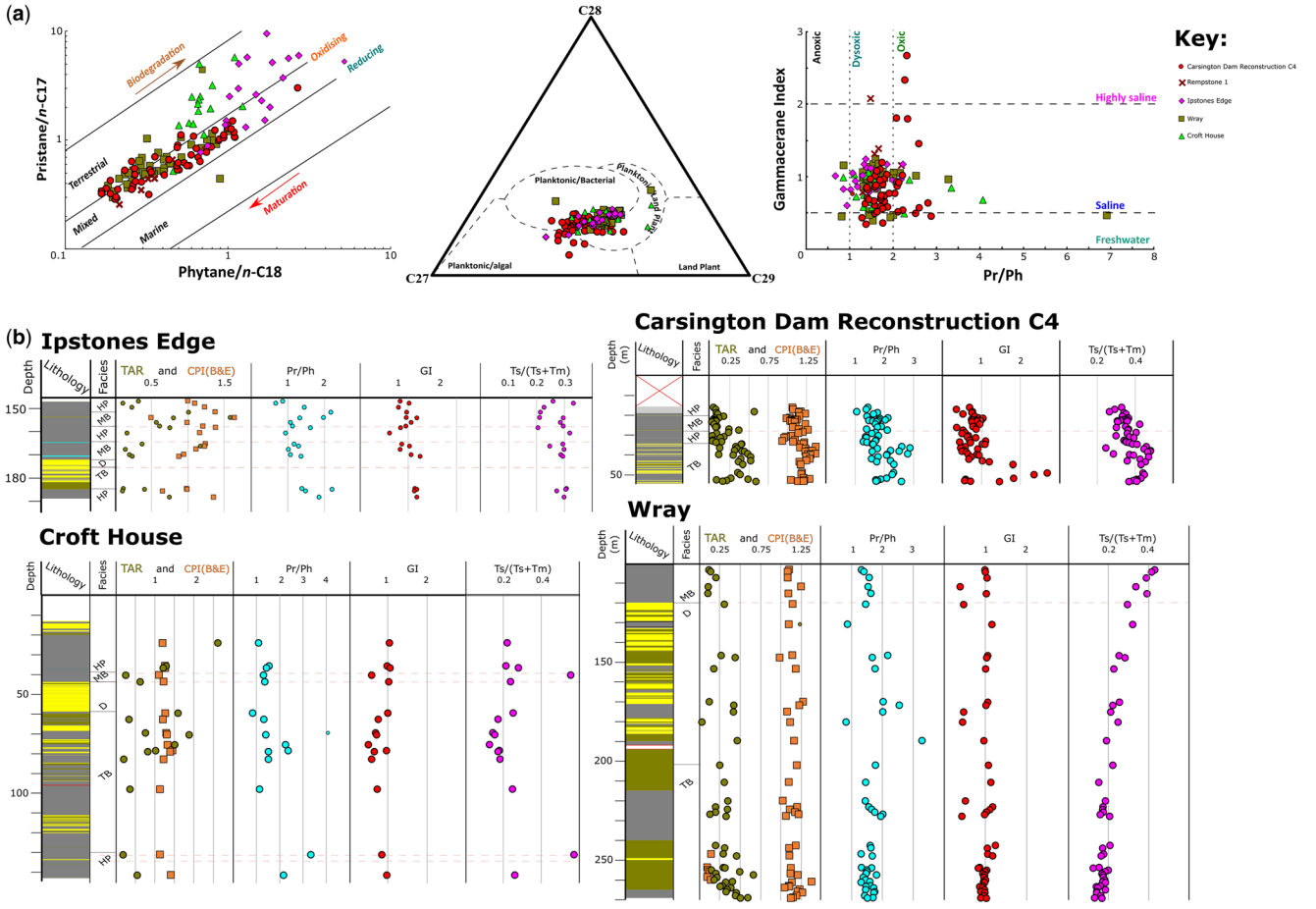

Fig. 5. (**a**) Biplots of biomarker indices (from left to right): pristane/n-C_{17} over phytane/n-C_{18} with organic matter type and depositional lines overlain, showing a similarly predominantly mixed kerogen type; ternary plot of sterane abundances drawn as in Figure 4 using the $C_{27–29}$ ααα*R* steranes to eliminate diasterane effects; plot of gammacerane index (GI) over Pr/Ph. Data clusters in the saline dysoxic zone as in Figure 4a; however, this dataset has more samples representing oxic saline conditions. (**b**) Logs of biomarkers in comparison to stratigraphy for the Arnsbergian-age sampling sites from the current study. The carbon preference index (CPI) is interpreted as in Figure 4b.

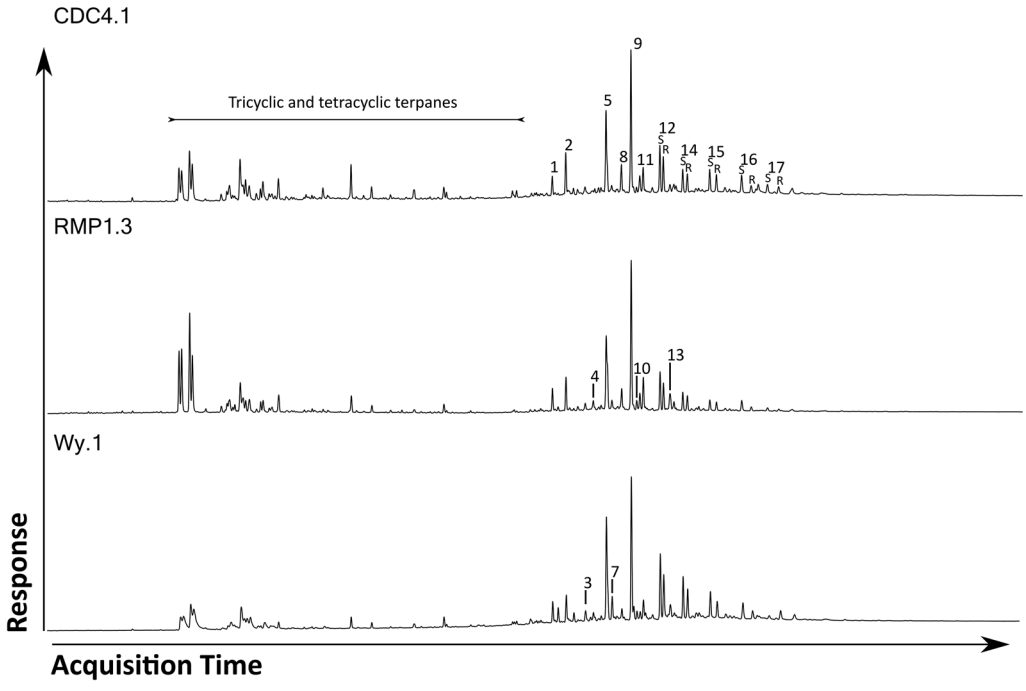

Fig. 6. GC-MS-SIM 191.1 plots of select samples from the dataset showing different distributions of terpanes. Labels are at the correct times for each chromatogram, and the numbers correspond to compounds listed in Table 1.

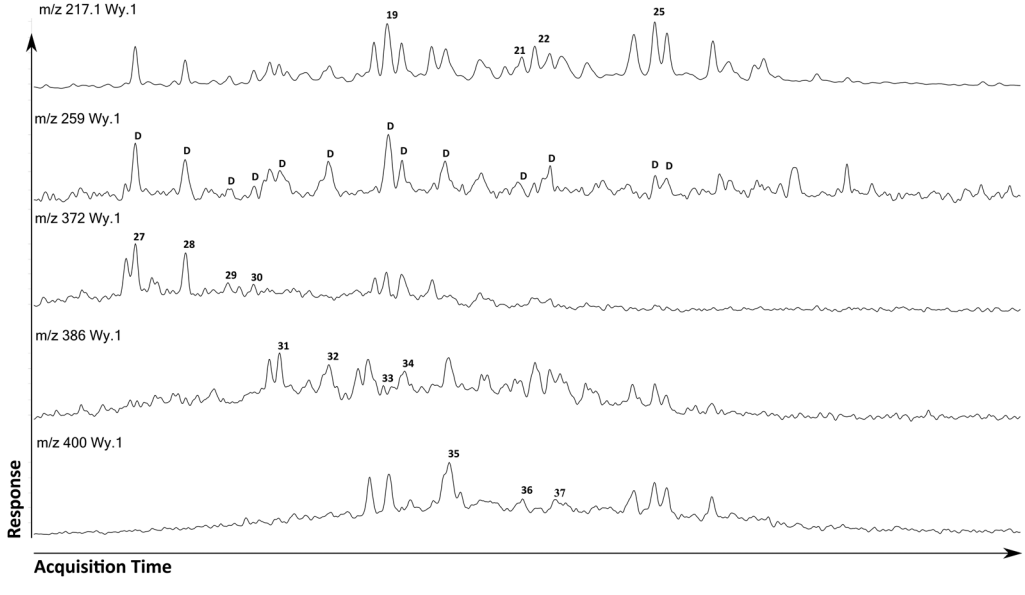

Fig. 7. GC-MS-SIM 217 and relevant extracted ion chromatograms (EICs) showing the $C_{27–29}$ sterane content. The m/z 217 EIC is labelled with regular sterane peaks that clearly coeluted with diasteranes. The m/z 259 EIC is labelled to show key diasterane peaks (D). The m/z 372–400 EICs are labelled with identified diasteranes found in the samples. Labels correspond to compounds in Table 1.

Table 1. *List of biomarkers and acronyms used for organic constituents found in this study*

Number assigned	Compound name	Acronym	Compound class	Carbon number
1	22,29,30-Trisnorneohopane	Ts	Trisnorhopane	27
2	22,29,30-Trisnorhopane	Tm	Trisnorhopane	27
3	17α(H)-Diahopane	C_{29}*	Diahopane	29
4	17α-norhopane	C_{28}Nor	Norhopane	28
5	17α,21β(H)-30-Norhopane	29αβ	Norhopane	29
6	18α(H)-30-Norneohopane	29Ts	Norneohopane	29
7	17α(H)-Diahopane	C_{30}*	Diahopane	30
8	17β,21α(H)-30-Norhopane (normoretane)	29βα	Moretane	29
9	17α,21β(H)-Hopane	H/30αβ	Hopanes	30
10	17α(H)-30-Nor-29-Homohopane	30Ts	Norneohopane	30
11	17β,21α(H)-Hopane (moretane)	30βα	Moretane	30
12S	17α,21β(H)-29-Homohopane 22S	C_{31}S	Homohopanes	31
12R	17α,21β(H)-29-Homohopane 22R	C_{31}R	Homohopanes	31
13	Gammacerane	G	N/A	30
14S	17α,21β(H)-29-Homohopane 22S	C_{32}S	Homohopanes	32
14R	17α,21β(H)-29-Homohopane 22R	C_{32}R	Homohopanes	32
15S	17α,21β(H)-29-Homohopane 22S	C_{33}S	Homohopanes	33
15R	17α,21β(H)-29-Homohopane 22R	C_{33}R	Homohopanes	33
16S	17α,21β(H)-29-Homohopane 22S	C_{34}S	Homohopanes	34
16R	17α,21β(H)-29-Homohopane 22R	C_{34}R	Homohopanes	34
17S	17α,21β(H)-29-Homohopane 22S	C_{35}S	Homohopanes	35
17R	17α,21β(H)-29-Homohopane 22R	C_{35}R	Homohopanes	35
18	5α(H),13α(H),17α(H)- Cholestane (S)	27αααS	Regular Steranes	27
19	5α(H),13β(H),17β(H)- Cholestane (S + R)	27αββR + 27αββS	Regular Steranes	27
20	5α(H),13α(H),17α(H)-Cholestane (R)	27αααR	Regular Steranes	27
21	5α(H),14α(H),17α(H) methylcholestane (S)	28αααS	Regular Steranes	28
22	5α(H),14β(H),17β(H) methylcholestane (S + R)	28αββR + 28αββS	Regular Steranes	28
23	5α(H),14α(H),17α(H) methylcholestane (R)	28αααR	Regular Steranes	28
34	5α(H),14α(H),17α(H) ethylcholestane (S)	29αααS	Regular Steranes	29
25	5α(H),14β(H),17β(H) ethylcholestane (S + R)	29αββR + 29αββS	Regular Steranes	29
26	5α(H),14α(H),17α(H) ethylcholestane (R)	29αααR	Regular Steranes	29
27	13β,17α(H)-Diacholestane (S)	27βαS	Diasteranes	27
28	13β,17α(H)-Diacholestane (R)	27βαR	Diasteranes	27
29	13α,17β(H)-Diacholestane (S)	27αβS	Diasteranes	27
30	13α,17β(H)-Diacholestane (R)	27αβR	Diasteranes	27
31	13β,17α(H)-Diacholestane (S)	28βαS	Diasteranes	28
32	13β,17α(H)-Diacholestane (R)	28βαR	Diasteranes	28
33	13α,17β(H)-Diacholestane (S)	28αβS	Diasteranes	28
34	13α,17β(H)-Diacholestane (R)	28αβR	Diasteranes	28
35	13β,17α(H)-Diacholestane (S)	29βαS	Diasteranes	29
36	13β,17α(H)-Diacholestane (R)	29βαR	Diasteranes	29
37	13α,17β(H)-Diacholestane (R)	29αβR	Diasteranes	29

samples towards C_{29}, which contributes a mean 43% of the total $C_{27–29}$ sterane homologue content. The C_{28} sterane accounts for the lowest percentile of the steranes analysed. C_{27} has a mean of *c.* 35% of the total sterane homologue content. In the ternary plots in Figures 4a and 5a the samples show a central distribution between C_{27} and C_{29}, which fits into a mixed planktonic/bacterial/land plant organic matter zone.

Comparison of the m/z 217 and 259 EICs in Figure 7 demonstrated that a number of peaks represent diasteranes, or a coeluted mix of steranes and diasteranes. Affected sterane peaks observed include but are not limited to 27αββR, 27αααS and 28αββR. The coelution of compounds reduced the accuracy of quantification, distorting indices reported from those peak areas. For the purposes of testing the impact of clay mineralogy on organic matter alteration, the ratio of 27βα (S + R) diasterane to 27αααR sterane was used in place of conventional ratios. This was due to the fact these peaks have been influenced the least by coelution. For comparison of sterane abundances the αααR sterane peak was used.

Some lower mass peaks visible in the m/z 217 EIC were tentatively assigned to the $C_{22–33}$

sterane/diasterane homologues, but were not interpreted in the current study. After the $C_{29}\alpha\alpha\alpha$20R sterane there are a number of peaks indicative of C_{30} steranes (Fig. 7). Interpretation of the C_{30} sterane peaks was tentative as the peaks coeluted with other compounds; thus they were not quantified for the current study.

Aryl isoprenoids and other observed aromatics

Peaks representing a suite of aryl isoprenoid compounds with carbon numbers from C_{11} to C_{27} were recognized through comparison of the m/z 133 and 134 EICs as in Figure 8. Peak areas for some of these compounds were quantified to produce the aryl isoprenoid ratio (AIR) after Schwark and Frimmel (2004), calculated as $(C_{13-17})/(C_{18-22})$. Of the 200 samples analysed through GC-MS methods, only 123 samples had aryl isoprenoid peaks. None of the samples from the Warlow Mires-1 and Cominco-S3 boreholes had quantifiable peaks, and only four samples from the Croft House core and 12 from Wray were quantifiable. The AIR across all measured samples ranges from 0.16 in the Ipstones Edge borehole to a maximum of 16.78 in the Carsington Dam Reconstruction-C4 borehole. Marl Hill and Lees Farm boreholes made up the lower range values, while Carsington Dam Reconstruction-C4 and Rempstone-1 contributed the most to the higher range. The precursor molecule for the aryl isoprenoids was not confirmed through isotope ratios; thus a β-carotane precursor cannot be ruled out. Neither β-carotane nor isoreniaretane were identified in any samples, and probably remain within the kerogen structure owing to the low maturity of material sampled.

As can be seen in Figure 8, the m/z 133 EIC shows a range of additional peaks alongside the aryl isoprenoids. Mass chromatograms were checked against other aromatic compounds, finding matches through the m/z 204 and 205 EICs showing coelution of C_{15} isohexyl alkylaromatics. Additionally, through the m/z 246 EIC phenylalkanes were observed, C_{18} phenylalkane in particular.

Mineralogy from XRD

The XRD analysis, as summarized in Figure 9, showed a primarily clay to silicate rich composition. Two samples from Carsington Dam Reconstruction-C4 plotted as being carbonate rich. The distribution of data points matches those published by Hennissen *et al.* (2017). Two mineralogical populations were determined. Arnsbergian samples from Rempstone-1, Wray and Carsington Dam Reconstruction-C4 were found to commonly contain a clay-rich and carbonate-poor mineralogy. The second population is made of samples from Carsington Dam Reconstruction-C4, Lees Farm-1 and Marl Hill-MHD4; this plots under a siliceous

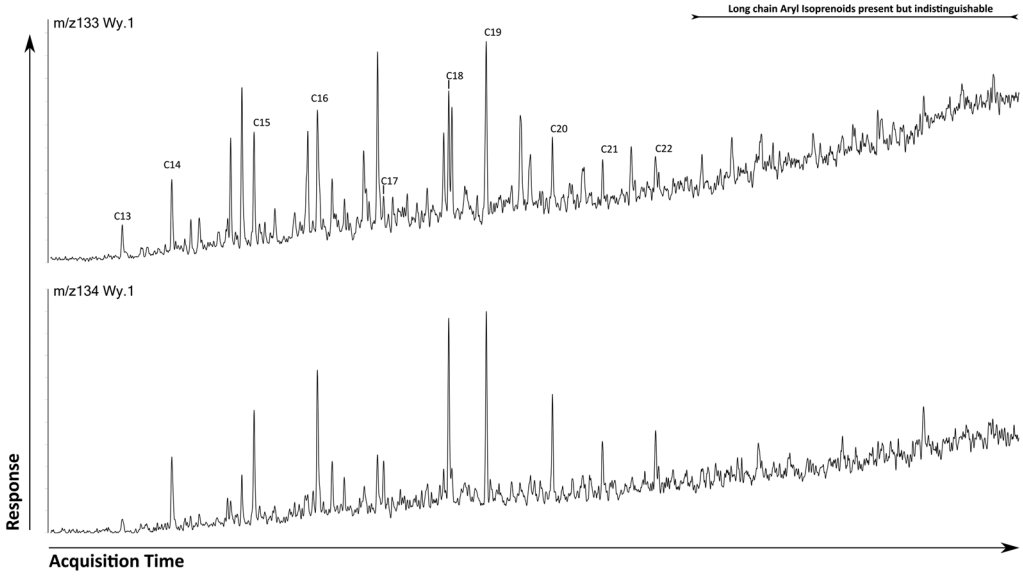

Fig. 8. Extracted ion chromatogram (EIC) of m/z 133 showing the distribution of aryl isoprenoids. The m/z 134 EIC was used to identify peaks, as the 133 EIC shows a range of additional unidentified aromatic compound peaks. Compounds are denoted by their carbon number as C*n*.

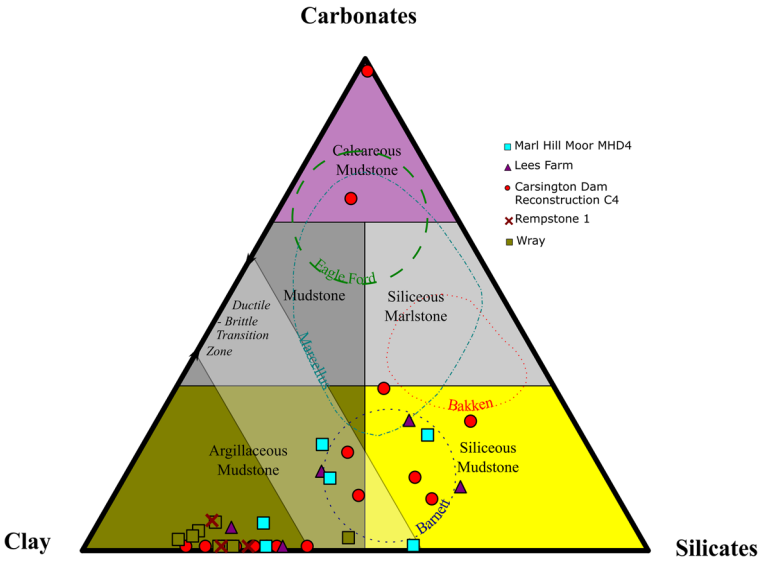

Fig. 9. Mineral ternary diagram after Hennissen *et al.* (2017), showing the distribution of Mississippian samples against mudstone classifications. Two groups of mudstone type were found. The first was highly argillaceous, comprised almost entirely of clay and silicate minerals. The second group is a more siliceous mudstone. Average areas for US Shale Plays after Mews *et al.* (2019) and references therein are also displayed; this showed a comparison between siliceous UK Carboniferous mudstones and the Barnett Formation suggesting that locations such as Lees Farm-1 and Marl Hill Moor-MHD4 are more suitable as a classic shale play.

mudstone category and matches average data for the Barnett Formation.

The clay mineral type comprises a mixture of expandable clays, classified through Profex as smectites combined with illite. Attempts to distinguish maturity levels were not possible owing to mixed layering of the expandable clay fraction. Kaolinite was commonly observed in the samples, but quantification was complicated as the peaks were shared with chlorite, which was mostly present in Arnsbergian-aged samples.

Carbonate mineralogy changes across the sample set dependent on location. Carsington Dam Reconstruction-C4 contained a mix of calcite and ankerite, which was also observed by Hennissen *et al.* (2017). Lees Farm was found to contain peaks correlating to dolomite. Marl Hill Moor-MHD4 contained only calcite. The Wray borehole only had calcite in two samples, which correlated to the marine band in the top of the cored section. Trace to 5% concentrations of siderite were observed in samples from Rempstone-1 and in turbidite facies belonging to the Wray borehole.

Pyrite was commonly measured in the samples. The highest pyrite contents were recorded in Marl Hill Moor-MHD4, which had a range from 1 to 11.64%. Pyrite was commonly associated with samples originating from marine facies. Very little pyrite was recorded in the Wray borehole, consistent with its common terrestrial kerogen classification. Anatase was also commonly observed in most samples but in low to trace abundances (<5%).

Discussion

Overall source rock potential from bulk geochemistry

The average TOC contents for the sampled cores may be defined as 'good' to 'very good' (Peters 1986), with the average values above the proposed cut-off of 2% by Andrews (2013). According to the S2/TOC biplots in Figures 2c and 3c only 40 samples fell below the 2% cut-off. However, the volume of TOC that can generate hydrocarbons has a greater significance to source rock potential than the presence of any TOC.

Correlation of TOC content and S2 (Figs 2c & 3c) shows that the samples from each basin distribute slightly differently. The Bowland basin samples have a significantly lower S2 to TOC correlation than the samples from the East Midlands. Overall, the majority of data points align with published data, with samples analysed in this study matching argillaceous/terrestrial organo-facies (Newport *et al.* 2018; Emmings *et al.* 2020*a*). The Arnsbergian-aged samples (Fig. 3c) closely matched trends from the

Duffield and Carsington Dam Reconstruction-C3 and C4 boreholes.

Our interpretation of the organic matter source from the S2–TOC plots in Figures 2c and 3c suggested that the samples were mostly composed of either 'mixed' type kerogens or Type III and IV. These kerogen types would not fit with the required standards for a shale play in the UK (Andrews 2013). HI–OI plots show that many of the samples plot close to the axis intercept for both sample sets, indicating a low generative potential (Fig. 2). This demonstrated some relationship to facies whereby samples from turbidite and hemipelagite facies had the lowest potential. Marine band facies were always found to have the highest HI to OI ratio. Data points typically follow the maturation trend lines for either Type II or Type III source rocks. Only a few samples exceed HI values of 300 mgHC g^{-1} TOC, which would make for a suitable shale gas target (Andrews 2013).

The poor generative potential represented by HI or S2 values demonstrated that the TOC content present had a low pyrolytic potential. Palynological analysis of the Carsington Dam Reconstruction-C4 borehole (Könitzer *et al.* 2016) interpreted that dispersed organic matter was distributed by suspension settling of granular amorphous material. The organic matter has been reported to represent biotic degraded organic matter with observation of aliphatic-rich material supported in faecal matter (Emmings *et al.* 2019). Newport *et al.* (2020) interpreted the Bowland Shale Formation of the Marl Hill-11 borehole to have a high oil yield from primary generation based on relative proportions of Type I and II kerogens. Modelling and pyrolysis experiments on kerogen extracts from the Widmerpool Gulf showed high primary generation and expulsion; however, secondary gas generation was regarded as a significant contribution to the hydrocarbon yield (Yang *et al.* 2016). Hennissen and Montesi (2020) observed fluorescence and Type I macerals such as *Botryococcus* sp. in Arnsbergian-aged rocks, which would support the argument that Carboniferous shales have a high primary oil producing capability. The above studies did not report significant quantities of inertinite matter, which could be regarded as a candidate for enhanced TOC contents in low S2 yield samples.

General environment of deposition

Information about the environment of deposition extracted from programmed pyrolysis data is uncertain, presenting difficulties with estimating kerogen type and generative potential. Studying the molecular representation of organisms (biomarkers) is a means to determine the environmental conditions under which a source rock was deposited.

Using Pr/Ph as a palaeoredox index (Didyk *et al.* 1978), the mean average of the sample set (1.55) falls within the 'dysoxic' window. Comparison of these acyclic isoprenoids and their *n*-alkane counterparts (Figs 4a & 5a) supports the dysoxic interpretation. The mean of the dataset is similar to averages from the Marl Hill-4 borehole (Emmings *et al.* 2020*a*), the Duffield borehole (Gross *et al.* 2015) and Malton-4 (Słowakiewicz *et al.* 2015), highlighting that reducing conditions were prevalent across the Carboniferous seaways present in northern England. Predominance of C_{31} over C_{35} hopane homologues seen from chromatographs can indicate sub-oxic to oxic conditions, although the ratio is impacted by thermal maturity and mineralogy (Peters and Moldowan 1991).

Identification of trace amounts of aryl isoprenoids supports the evidence that reducing conditions were present and contributed to the water column chemistry (Fig. 10). Reducing conditions detected via low Pr/Ph supported more stable photic zone euxinia, evidenced by a prevalence of long-chain aryl isoprenoids in Figure 10 (Schwark and Frimmel 2004). Evidence of combined dysoxia and euxinia refers to zonation in the water column. During deposition, a thicker euxinic water column would have been present, representing poor ventilation of bottom waters. Organic matter produced by surface productivity was decomposed by sulfate-reducing bacteria at the sediment–water interface, recognized from samples at Marl Hill-4 (Emmings *et al.* 2020*a*). Samples representing more oxidizing environments in Figure 10 showed a predominance of shorter-chain aryl isoprenoids indicating that at locations where they could be detected, photic zone anoxia was likely to be episodic and organic matter was exposed to oxidative degradation for extended periods of time (Schwark and Frimmel 2004). Group 1 represents marine facies, i.e. marine bands, hemipelagite and carbonate slope, all associated with indicators of persistent euxinia extending to the photic zone. Turbidite facies form Group 2 on Figure 10, representing episodic photic zone anoxia consistent with ventilation of the water column during lowstand sea levels (Gross *et al.* 2015; Emmings *et al.* 2020*a*). Ventilation of the water column enabled degradation of the aryl isoprenoid chains (Schwark and Frimmel 2004) probably during the same periods that contributed to microbial sediment–water interface effects as in Emmings *et al.* (2020*b*).

Gammacerane supports the interpretation of a stratified water column (Sinninghe Damste *et al.* 1995); however, the values do not vary significantly through the dataset and no major peaks were detected from the 191 EICs. Gammacerane is commonly associated with bacteriovorous ciliates living beneath chemoclines (Harvey and McManus 1991; Sinninghe Damste *et al.* 1995) often connected

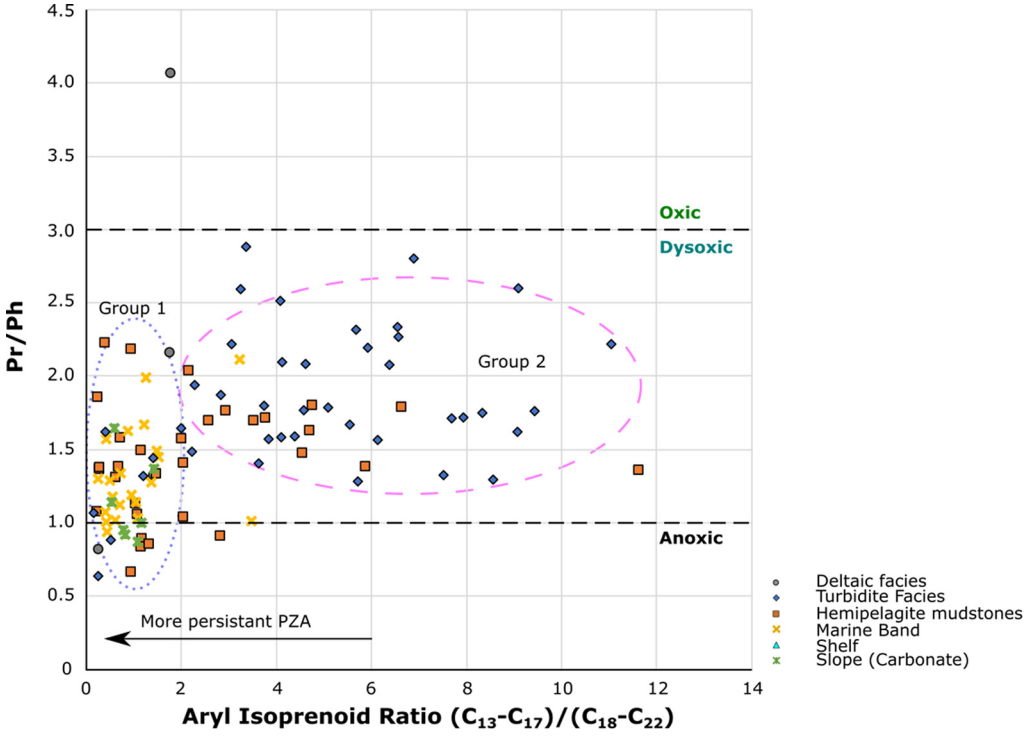

Fig. 10. Cross-plot of Pr/Ph over aryl isoprenoid ratio (AIR). The trend has a positive correlation (after Schwark and Frimmel (2004)), this indicates that samples towards the axis intercept have persistent photic zone anoxia (PZA) conditions. Samples with relatively higher Pr/Ph and AIR have more episodic conditions. Samples have been sorted by the facies type from Figures 2 to 5 to highlight trends from the relative environmental conditions of deposition. Two groups were identified: Group 1 relates to marine type facies, i.e. carbonate slope, marine bands and hemipelagite, which demonstrate enhanced reducing deposition; Group 2 primarily consists of the turbidite facies, which would be deposited under episodic conditions.

with, but not limited to, hypersaline environments (Peters *et al.* 2005). The concentrations reported in the current study do not provide evidence for hypersaline conditions. Other influences must have generated stratification, i.e. thermal layering (Emmings *et al.* 2020*a*). GI v. Pr/Ph in Figure 4a shows that there is a slight relationship between Pendleian–Brigantian reducing conditions and water column salinity. Most samples shown in Figure 5a suggest that dysoxic saline conditions prevailed during the Arnsbergian.

From 51.6 m in the Carsington Dam Reconstruction-C4 log there is a significant excursion of GI values. This is following from the proposed location of the $E_{2a}2b$ marine band at 52.6–53.1 m (Brandon *et al.* 1995; Könitzer *et al.* 2014). Gross *et al.* (2015) provided no data or interpretation on that minor cycle. The excursion coincides with the onset of low sea-level conditions and deposition of distal turbidites potentially connected to the uppermost Duffield Turbidite (Aitkenhead 1977). Könitzer *et al.* (2014) described bioturbated and lenticular facies indicating enhanced sediment–water interface oxygenation, proven here by relatively higher Pr/Ph. The excursion is interpreted as being representative of sea-level fall and the development of a substantial oxygenated freshwater lens across saline bottom waters in the Widmerpool Gulf. This is the only significant salinity stratification observed from the gammacerane data in the current study. Aryl isoprenoids were detected in this layer, with a relatively high AIR, ranging from 3.05 to 8.33, plotting in Group 2 on Figure 10. Any anoxia present would have been highly episodic with a ventilated water column; anoxia would have been driven by productivity in the surface-water layer (Emmings *et al.* 2020*b*).

Origin of organic matter

Most samples have a Pr/*n*-C_{17} and Ph/*n*-C_{18} ratio of <1, which in this case was interpreted as being representative of an algal or microbial short-chain alkane origin, as was suggested for the Duffield

borehole by Gross *et al.* (2015). Such a trend could be generated by maturity, but would not be expected within early oil window samples. Analysis of the distribution of the *n*-alkanes further supports the aquatic organic constituent source. The TARs reported in Figures 4b and 5b are <1 indicating an aquatic origin. Meanwhile the CPI is *c.* 1 for many samples, indicative of marine conditions and no preference in chain length. Locations such as Wray, Croft House and Rempstone have slightly higher CPI value distributions (>1), which would be consistent with a terrestrial organic contribution represented by the deltaic derived detrital sandstones logged from the core material available. The tentative observation of C_{30} sterane peak areas in the samples is further evidence for a marine organic source (Moldowan *et al.* 1985; Peters 1986).

Predominance of the C_{29} sterane isomers over other sterane groups in the samples was interpreted to be representative of terrestrial organic matter (Volkman 1986). However, the samples relate to a planktonic/bacterial/land plant window suggestive of organic mixing. Some of the potential aromatic molecule candidates present alongside the aryl isoprenoids on the m/z 133 EIC could be representative of isohexyl alkylbenzenes such as $C_{15}H_{24}$ 1,3,4-trimethyl-2-(4-methylpentyl) benzene. Isohexyl alkylbenzenes are indicative of higher plant or microbial input (Wang *et al.* 1990; Ellis *et al.* 1996), both of which are viable explanations based on the organic macerals representing bacterial degradation of terrestrial matter described by Könitzer *et al.* (2016).

In agreement with observations from Gross *et al.* (2015), the general organic source was mixed. Algal and bacterial markers such as short-chain alkanes, tricyclic terpanes and C_{27} steranes provide a strong indicator of organic matter akin to Type II kerogens. This interpretation is consistent with palynological observation (Könitzer *et al.* 2016; Hennissen *et al.* 2017; Newport *et al.* 2020) and interpretation of the source rock activation energies (Yang *et al.* 2016; Newport *et al.* 2020). C_{29} steranes present evidence of terrestrial organic matter that was biotically decomposed as it settled through a stratified water column. Samples from the Widmerpool Gulf show greater variation in the ratio of C_{27} to C_{29} than their counterparts in the Craven Basin (Figs 4a & 5a). Extracted steranes from the Craven Basin express a slight preference towards C_{29}, which is probably generated by proximity to the Pennine Delta front and the resultant consistency of terrestrial organic matter influx and preservation.

Maturity indices and influencing factors

Based on the average T_{max} trends for the boreholes in Figures 2b and 3b, the samples analysed in this study are early oil to peak oil mature. This is supported by low vitrinite reflectance (% R_o) values for locations such as 0.55% R_o at Rempstone-1 (Coombes *et al.* 1986; Hennissen and Gent 2019), a calculated % R_o of 0.5–0.8 at the Carsington Dam locality (Henry *et al.* 2018) and similarly the Marl Hill locality's calculated % R_o of 0.8 (Herrmann *et al.* 2018). Some boreholes exhibited anomalous T_{max} ranges that were inconsistent with the geothermal gradient and burial depth range of the sampled interval; for example, Cominco-S3 in Figure 2b has a T_{max} range of 20°C in the upper 20–30 m of the cored section. As the samples are within the oil window, they are not interpreted directly as a shale gas resource and should not exhibit such high maturities.

Biomarkers also provide maturity data, through effects such as preferential thermal degradation or isomerism of compounds. Figure 11 shows

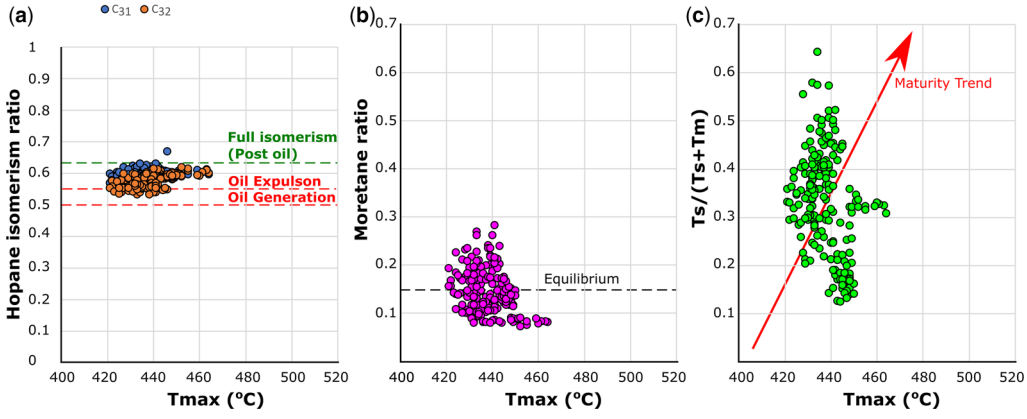

Fig. 11. Cross-plots of common biomarker maturity indices against T_{max} recorded from programmed pyrolysis. (**a**) Hopane isomers. (**b**) Moretane ratio, calculated from hopane values as $30\beta\alpha/(30\beta\alpha + 30\alpha\beta)$. (**c**) Ts/(Ts + Tm); the red arrow shows the anticipated maturity trend for this biomarker.

biomarker maturity indices plotted against T_{max}, revealing a range of either correlating or contradicting relationships. Firstly, the hopane inventory (Fig. 11a) of the samples had reached hopane isomer equilibrium, indicating that the source rocks were at an oil expulsion maturity level. Moretane ratios were also determined to have achieved full maturity with no apparent relationship to T_{max}. However, Ts/Tm (Fig. 11c) shows no T_{max} relationship and a low to moderate maturation level.

Influences from the environment of deposition are the most likely cause of these trends. The moretane ratios indicate a predominance of C_{30} hopane over moretane. Rullkötter and Marzi (1988) observed high moretane values in hypersaline rocks, while Isaksen and Bohacs (1995) observed enhanced moretane ratios in highstand as opposed to lowstand tracts, which was attributed to higher plant contributions. It would be reasonable to expect such a trend in the Carboniferous mudstones. However, the generation of moretane can also be attributed to bacteria in oxidizing sediments as well as diagenetic effects under certain clay types (Quirk *et al.* 1984; Uemura and Ishiwatari 1995; Wang 2007; French *et al.* 2012).

A predominance of Tm over Ts may relate to either immaturity, oxidizing environments or variations in clay influence (McKirdy *et al.* 1983; Waples and Machihara 1990; Peters *et al.* 2005; French *et al.* 2012). Figure 11c shows no relationship between T_{max} and Ts/Tm, highlighting the low maturity of the samples and emphasizing that alternative influences must have a control on the ratio. Ts/Tm has a complex relationship with Pr/Ph. In the Wray geothermal borehole (Fig. 5b), Ts/Tm increases above the E_{2b} marine band indicating enhanced reducing conditions at the sediment–water interface. This is likely to be connected to sulfate reduction during flooding of shelf or delta proximal areas as suggested by Emmings *et al.* (2020*a*). In the Widmerpool Gulf at the Carsington Dam Reconstruction-C4 locality, samples above the E_{2b} marine band have a reduced Ts/Tm correlating with reduced Pr/Ph consistent with a switch to carbonate pH effects in porewater (Fig. 1) (Moldowan *et al.* 1994). The Pendleian–Brigantian samples in Figure 3b show elevated Ts/Tm ratios consistent with widespread Eh effects in porewater during the Mississippian. Carbonate influences are demonstrated in the lower 10 m of Wardlow Mires.

Figure 12a highlights three populations of samples based on the relationship of Ts/Tm and diasteranes. Group 1 represents anoxic marine conditions whereby organic matter is deposited under euxinic conditions with a moderate flux of detrital clays during marine band and highstand sea-levels. Group 2 represents deposition under dysoxic to oxic conditions with samples commonly representing prodelta depositional conditions. Group 3 was defined by the presence of slope, hemipelagite and marine band conditions, representing a setting in which marine organic matter is deposited under euxinia alongside clay input.

The ratio of C_{27} diasteranes to 27ααα*R* steranes corelates positively to the full range of T_{max} values (Fig. 12b). As opposed to a maturity relationship, the corelation is representative of a mineral matrix effect on programmed pyrolysis results (Espitalié 1986; Peters 1986). The influence interpreted in the current study involved adsorption of free hydrocarbons onto mineral surfaces, decreasing pyrogram peaks and leading to a T_{max} shift to high temperatures or poor quality S2 peaks (Espitalié *et al.* 1984; Hu *et al.* 2014; Yang and Horsfield 2020). Research has suggested that samples with TOC contents over 2 wt% (Dembicki 1992) and over 0.2 mgHC g^{-1} rock S2 values (Peters 1986) should not be susceptible to the mineral matrix effect. However, data in the current study and palynological data originally observed by Könitzer *et al.* (2016) demonstrated that not all of the TOC is necessarily generative owing to biotic decomposition, and the generative fraction can therefore be overwhelmed by the mineral surfaces.

Different facies types relate to diasterane/T_{max} trends. Turbidite facies representative of prodeltaic deposition have a strong positive correlation representative of the influence of clay minerals on pyrolysis results. Facies associated with terrestrial organic matter such as deltaic shelf sediments have the highest T_{max} results, which was also observed in Emmings *et al.* (2020*a*). Marine bands and hemipelagite facies show a lower influence by clay minerals on T_{max} maturity; the trends tend to reverse at boundaries between facies in Figures 3 and 4.

Hopane isomers, in particular the C_{31} and C_{32} homologues typically studied in the samples, have reached equilibrium (Fig. 11a, c) (Peters *et al.* 2005). The C_{31} isomer ratios in Figure 12c positively correlate with the diasterane ratios used. Fully isomerized hopane homologues in immature sediments have been observed in other basins, i.e. by Moldowan *et al.* (1992) or ten Haven *et al.* (1986). Laboratory experimentation has in the past demonstrated high hopane isomer ratios that can be 'reset' during laboratory pyrolysis (Peters *et al.* 1990), suggesting that high values can be altered by expulsion. Hopane release is in part controlled by the breaking of sulfur bonds from kerogen (Köster *et al.* 1997), the nature of which may complicate the ratio. Corelation with diasteranes is indicative of a mineral catalytic effect or relates to the environment of deposition in a stratified water column that enabled sulfur incorporation into organic mediums. Emmings *et al.* (2020*a*) reported sulfidic conditions and shallow precipitation of pyrite framboids under highstand sea-level

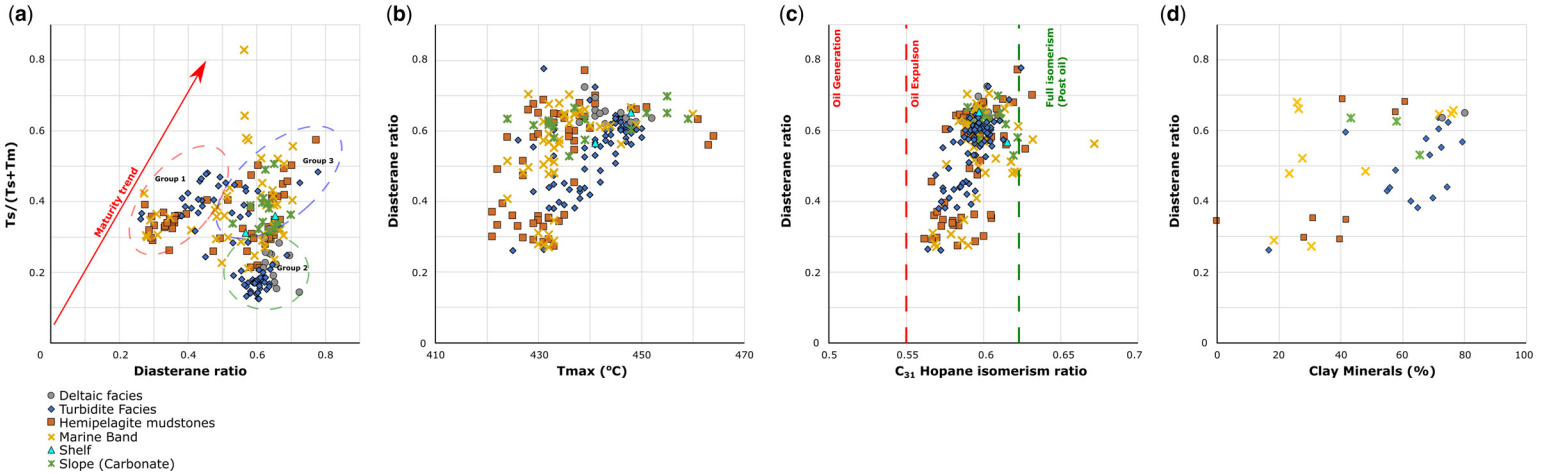

Fig. 12. (**a**) Plot of Ts/Tm v. C_{27} diasterane ratio; an approximate maturity trend would be positive and linear, which is represented by the red arrow. The effect of oxidation produces an orthogonal trend to maturity demonstrated by samples with a low Ts/Tm and higher diasterane ratio. (**b**) Diasteranes plotted v. T_{max} show that as T_{max} increases so do rearranged steranes, which would normally by indicative of maturation. However, the boreholes have such a range of T_{max} values over short periods that a mineral matrix effect is deduced to have created such a trend. (**c**) The ratios of hopane isomers for C_{31} homohopanes against the diasterane ratio. The linear trend is indicative that controls on T_{max} and diasterane distribution also effect the ratio of hopane isomers, demonstrating the significance of mineral matrix effects. (**d**) Correlation of diasteranes to per cent abundance of clay minerals identified through XRD analysis. A positive relationship was found, which indicates a connection between clay deposition and organic preservation or alteration. Turbidite facies samples have the highest diasterane ratio and clay mineral contents, while hemipelagic facies samples have the lowest of both. Interestingly, marine band facies samples show variability, and thus other chemical effects might be the cause of the relationship.

conditions; the fully isomerized hopanes in marine band and hemipelagite facies associated with diasteranes may be indicative of sulfur bond influences relating to the observations. In the current study, pyrite concentrations were found to be highest in the marine band or hemipelagite facies, further supporting this. In the case of turbidite facies, the observed ratio most probably relates to clay catalysis of organic matter. This is supported as turbidite facies plot with the highest clay mineral percentages and diasterane ratios (Fig. 12d). Hemipelagite type mudstones plotted with a lower clay to diasterane relationship, while marine bands were more distributed in Figure 12d, reinforcing that Eh to pH effects have a greater influence for those facies.

Studies employing equations to calculate % R_o equivalent from T_{max} (using the linear regression modelling) need to consider if the T_{max} result is likely to be increased by the mineral matrix effect giving inaccurate maturity trends. Studies such as Andrews (2013) specifically incorporated conversions to establish burial curves for the Upper and Lower Bowland Shale. To counter mineral matrix effects, Yang *et al.* (2016) recommended use of kerogen isolates, but the potential of a diagenetic mineral matrix effect on oil window organic matter means that the compositional kinetic pathways of yields from kerogen isolates may be inaccurate and not reflective of the true timing of generation v. expulsion.

Maturity results for the Bowland Shale and its diachronous counterparts have been largely misinterpreted in the literature, and care should be taken when using these to aid petrophysical calculations as in Hennissen and Gent (2019). Owing to the advanced ratios of certain biomarkers, the samples described in the current study are in the early to mid oil window with an equivalent vitrinite maturity of 0.7 to 0.8% R_o (Peters *et al.* 2005). Low T_{max} results in marine band facies were generated by mineral retention effects, and high values in low sea-level facies were influenced by the refractory oxidized organic macerals preserved.

Conclusions

The water column conditions as represented by EOM within the Mississippian basins of northern England are characterized by a continuous dysoxic layer between the sediment–water interface extending euxinia into the photic zone. Influx of terrigenous organic matter and settling of marine organic matter into the basin is proposed to have acted as a feedstock for a bacterial food web, leading to the preservation of compounds related to these groups, i.e. terpanes, hopanes and gammacerane. The high nutrient load into the basins encouraged the establishment of reducing conditions and switching to sulfate reduction. The kerogen type interpreted from the EOM is a mixed type, but hydrocarbon generative potential at marine band and highstand sea-level periods would be akin to Type II kerogens despite the mixing.

A mineral matrix effect influences both naturally and pyrolytically matured samples from the current study. Authors using programmed pyrolysis to interpret source rock hydrocarbon prospectivity or to calculate the original parameters should be aware that key values deriving S1 and S2 peaks will be reduced. Further work on hydrous, anhydrous and programmed pyrolysis exploring the role of pyrolysable v. residual carbon in hydrocarbon generation will be required to deduce the importance of this effect for this particular formation. The results of such studies have application in the wider exploration of deltaic-derived source rocks where detrital minerals and organic matter are deposited and matured together.

Acknowledgements The work contained in this paper contains work conducted during a PhD study undertaken as part of the Natural Environment Research Council (NERC) Centre for Doctoral Training (CDT) in Oil & Gas. Samples were provided by the British Geological Survey (BGS), with special thanks given to the Core Store for provision of facilities, time and understanding. Finally, the two anonymous reviewers along with editors Bhavik H. Lodhia and Joseph F. Emmings are thanked for their comments and suggestions during the preparation of the work.

Competing interests The authors declare that they have no known competing financial interests or personal relationships that could have appeared to influence the work reported in this paper.

Author contributions **MJES**: conceptualization (lead), formal analysis (lead), methodology (lead), writing – original draft (lead); **MAS**: funding acquisition (lead), methodology (supporting), project administration (supporting), resources (lead), supervision (lead), writing – review & editing (lead); **JSW**: methodology (equal), writing – review & editing (supporting); **AJF**: funding acquisition (equal), project administration (equal), supervision (equal), writing – review & editing (equal); **CHV**: resources (supporting).

Funding This work was supported by the Natural Environment Research Council (NERC) Centre for Doctoral Training (CDT) in Oil & Gas [grant number NEM00578X/1] and completed as part of the Natural Environment Research Council funded Unconventional Hydrocarbons in the UK Energy System project [grant number NE/R018065/1].

Data availability All data generated or analysed during this study are included in this published article (and its supplementary information files).

References

Agilent Technologies Inc. 2016. *Mass Hunter* version B.08.00. Agilent Technologies Inc.

Aitkenhead, N. 1977. The Institute of Geological Sciences borehole at Duffield, Derbyshire. *Geological Survey of Great Britain, Bulletin*, **59**, 1–38.

Algeo, T.J. and Li, C. 2020. Redox classification and calibration of redox thresholds in sedimentary systems. *Geochimica et Cosmochimica Acta*, **287**, 8–26, https://doi.org/10.1016/j.gca.2020.01.055

Andrews, I.J. 2013. *The Carboniferous Bowland Shale Gas Study: Geology and Resource Estimation*. British Geological Survey for Department of Energy and Climate Change, London.

Brandon, A., Riley, N.J., Wilson, A.A. and Ellison, R.A. 1995. Three new early Namurian (E_{1c}-E_{2a}) marine bands in central and northern England, UK, and their bearing on correlations with the Askrigg Block. *Proceedings of the Yorkshire Geological Society*, **50**, 333–355, https://doi.org/10.1144/pygs.50.4.333

Brandon, A., Aitkenhead, N., Crofts, R.G., Ellison, R.A., Evans, D.J. and Riley, N.J. 1998. *Geology of the Country around Lancaster*. Memoirs of the British Geological Survey, Sheet 59.

Bray, E.E. and Evans, E.D. 1961. Distribution of *n*-paraffins as a clue to recognition of source beds. *Geochimica et Cosmochimica Acta*, **22**, 2–9, https://doi.org/10.1016/0016-7037(61)90069-2

Breck, W.G. 1974. Redox levels in the sea. *In*: Goldberg, E.D. (ed.) *The Sea: Ideas and Observations on Progress in the Study of the Seas*. Vol. **5**. Wiley, New York, 153–179.

Chisholm, J.I., Charsley, T.J. and Aitkenhead, N. 1988. *Geology of the Country around Ashbourne and Cheadle*. Memoirs of the British Geological Survey, Sheet 124 (England and Wales).

Clarke, H., Turner, P., Bustin, R.M., Riley, N. and Besly, B. 2018. Shale gas resources of the Bowland Basin, NW England: a holistic study. *Petroleum Geoscience*, **24**, 287–322, https://doi.org/10.1144/petgeo2017-066

Coombes, D., Hughes, J., Maile, C.N. and Batten, D.J. 1986. *A Geochemical Evaluation of Sediment and Oil Samples from the Well Rempstone-1, East Midlands, UK Land*. BP Research Centre, Sunbury-on-Thames.

Degen, T., Sadki, M., Bron, E., König, U. and Nénert, G. 2014. The HighScore suite. *Powder Diffraction*, **29**, S13–S18, https://doi.org/10.1017/S0885715614000840

Dembicki, H., Jr 1992. The effects of the mineral matrix on the determination of kinetic parameters using modified Rock Eval pyrolysis. *Organic Geochemistry*, **18**, 531–539, https://doi.org/10.1016/0146-6380(92)90116-F

Didyk, B.M., Simoneit, B.R.T., Brassell, S.T. and Eglinton, G. 1978. Organic geochemical indicators of palaeoenvironmental conditions of sedimentation. *Nature*, **272**, 216–222, https://doi.org/10.1038/272216a0

Döbelin, N. and Kleeberg, R. 2015. Profex: a graphical user interface for the Rietveld refinement program BGMN. *Journal of Applied Crystallography*, **48**, 1573–1580, https://doi.org/10.1107/S1600576715014685

Ellis, L., Singh, R.K., Alexander, R. and Kagi, R.I. 1996. Formation of isohexyl alkylaromatic hydrocarbons from aromatization-rearrangement of terpenoids in the sedimentary environment: a new class of biomarker. *Geochimica et Cosmochimica Acta*, **60**, 4747–4763, https://doi.org/10.1016/S0016-7037(96)00281-5

Emmings, J.F., Hennissen, J.A. *et al*. 2019. Controls on amorphous organic matter type and sulphurization in a Mississippian black shale. *Review of Palaeobotany and Palynology*, **268**, 1–18, https://doi.org/10.1016/j.revpalbo.2019.04.004

Emmings, J.F., Poulton, S.W. *et al*. 2020*a*. A Mississippian black shale record of redox oscillation in the Craven Basin, UK. *Palaeogeography, Palaeoclimatology, Palaeoecology*, **538**, https://doi.org/10.1016/j.palaeo.2019.109423

Emmings, J.F., Davies, S.J., Vane, C.H., Moss-Hayes, V. and Stephenson, M.H. 2020*b*. From marine bands to hybrid flows: sedimentology of a Mississippian black shale. *Sedimentology*, **67**, 261–304, https://doi.org/10.1111/sed.12642

Espitalié, J. 1986. Use of Tmax as a maturation index for different types of organic matter: comparison with vitrinite reflectance. *In*: Burrus, J. (ed.) *Thermal Modelling in Sedimentary Basins*. Editions Technip, Paris, 475–496.

Espitalié, J., Madec, M., Tissot, B., Mennig, J.J. and Leplat, P. 1977. Source rock characterization method for petroleum exploration. Paper presented at the Offshore Technology Conference, 1–4 May 1977, Houston, Texas, https://doi.org/10.4043/2935-MS

Espitalié, J., Marquis, F. and Barsony, I. 1984. Geochemical logging. *In*: Voorhees, K.J. (ed.) *Analytical Pyrolysis*. Butterworth-Heinemann, 276–304.

Fraser, A.J. and Gawthorpe, R.L. 1990. Tectonostratigraphic development and hydrocarbon habitat of the Carboniferous in northern England. *Geological Society, London, Special Publications*, **55**, 49–86, https://doi.org/10.1144/GSL.SP.1990.055.01.03

Fraser, A.J. and Gawthorpe, R.L. (eds) 2003. *An Atlas of Carboniferous Basin Evolution in Northern England*. Geological Society, London, Memoirs, **28**, https://doi.org/10.1144/GSL.MEM.2003.028

French, K.L., Tosca, N.J., Cao, C. and Summons, R.E. 2012. Diagenetic and detrital origin of moretane anomalies through the Permian–Triassic boundary. *Geochimica et Cosmochimica Acta*, **84**, 104–125, https://doi.org/10.1016/j.gca.2012.01.004

Gross, D., Sachsenhofer, R.F., Bechtel, A., Pytlak, L., Rupprecht, B. and Wegerer, E. 2015. Organic geochemistry of Mississippian shales (Bowland Shale Formation) in central Britain: implications for depositional environment, source rock and gas shale potential. *Marine and Petroleum Geology*, **59**, 1–21, https://doi.org/10.1016/j.marpetgeo.2014.07.022

Harvey, H.R. and Mcmanus, G.B. 1991. Marine ciliates as a widespread source of tetrahymanol and hopan-3β-ol in sediments. *Geochimica et Cosmochimica Acta*, **55**, 3387–3390, https://doi.org/10.1016/0016-7037(91)90496-R

Hennissen, J.A. and Gent, C.M. 2019. Total organic carbon in the Bowland-Hodder Unit of the southern

Widmerpool Gulf: a discussion. *Journal of Petroleum Science and Engineering*, **178**, 1194–1202, https://doi.org/10.1016/j.petrol.2019.01.097

Hennissen, J.A. and Montesi, G. 2020. Quantitative palynological analysis of the E_{2a} and E_{2b} goniatite biozones (Arnsbergian, Mississippian) in mudstones from the Southern Pennine Basin (U.K.). *Review of Palaeobotany and Palynology*, **276**, 104187, https://doi.org/10.1016/j.revpalbo.2020.104187

Hennissen, J.A., Hough, E., Vane, C.H., Leng, M.J., Kemp, S.J. and Stephenson, M.H. 2017. The prospectivity of a potential shale gas play: an example from the southern Pennine Basin (central England, UK). *Marine and Petroleum Geology*, **86**, 1047–1066, https://doi.org/10.1016/j.marpetgeo.2017.06.033

Henry, D.G., Jarvis, I., Gillmore, G., Stephenson, M. and Emmings, J.F. 2018. Assessing low-maturity organic matter in shales using Raman spectroscopy: effects of sample preparation and operating procedure. *International Journal of Coal Geology*, **191**, 135–151, https://doi.org/10.1016/j.coal.2018.03.005

Herrmann, J., Rybacki, E., Sone, H. and Dresen, G. 2018. Deformation experiments on Bowland and Posidonia Shale – part I: strength and Young's modulus at ambient and in situ p_c–T conditions. *Rock Mechanics and Rock Engineering*, **51**, 3645–3666, https://doi.org/10.1007/s00603-018-1572-4

Hu, M., Cheng, Z., Zhang, M., Liu, M., Song, L., Zhang, Y. and Li, J. 2014. Effect of calcite, kaolinite, gypsum, and montmorillonite on Huadian oil shale kerogen pyrolysis. *Energy & Fuels*, **28**, 1860–1867, https://doi.org/10.1021/ef4024417

Isaksen, G.H. and Bohacs, K.M. 1995. Geological controls of source rock geochemistry through relative sea level; Triassic, Barents Sea. *In*: Katz, B.J. (ed.) *Petroleum Source Rocks*. Springer, Berlin, 25–50.

Jarvie, D.M. 2012. Shale resource systems for oil and gas: part 1 – shale-gas resource systems. *AAPG Memoirs*, **97**, 69–87, https://doi.org/10.1306/13321446M973489

Kirby, G.A., Baily, H. *et al*. 2000. *The Structure and Evolution of the Craven Basin and Adjacent Areas*. British Geological Survey, Keyworth, Nottingham, 1–114.

Könitzer, S.F., Davies, S.J., Stephenson, M.H. and Leng, M.J. 2014. Depositional controls on mudstone lithofacies in a basinal setting: implications for the delivery of sedimentary organic matter. *Journal of Sedimentary Research*, **84**, 198–214, https://doi.org/10.2110/jsr.2014.18

Könitzer, S.F., Stephenson, M.H., Davies, S.J., Vane, C.H. and Leng, M.J. 2016. Significance of sedimentary organic matter input for shale gas generation potential of Mississippian Mudstones, Widmerpool Gulf, UK. *Review of Palaeobotany and Palynology*, **224**, 146–168, https://doi.org/10.1016/j.revpalbo.2015.10.003

Köster, J., Van Kaam-Peters, H.M., Koopmans, M.P., De Leeuw, J.W. and Damsté, J.S.S. 1997. Sulphurisation of homohopanoids: effects on carbon number distribution, speciation, and 22S22R epimer ratios. *Geochimica et Cosmochimica Acta*, **61**, 2431–2452, https://doi.org/10.1016/S0016-7037(97)00110-5

Lafargue, E., Marquis, F. and Pillot, D. 1998. Rock-Eval 6 applications in hydrocarbon exploration, production, and soil contamination studies. *Revue de l'Institut Français du Pétrole*, **53**, 421–437, https://doi.org/10.2516/ogst:1998036

Leeder, M.R. 1988. Recent developments in Carboniferous geology: a critical review with implications for the British Isles and NW Europe. *Proceedings of the Geologists' Association*, **99**, 73–100, https://doi.org/10.1016/S0016-7878(88)80001-4

Lodhia, B.H., Parent, A., Fraser, A.J., Nuemaier, M. and Hennissen, J. 2023. Thermal evolution and resources of the Bowland Basin (NW England) from apatite fission-track analyses and multidimensional basin modelling. *Geological Society, London, Special Publications*, **534**, https://doi.org/10.1144/SP534-2022-15

Maynard, J.R., Hofmann, W., Dunay, R.E., Benthan, P.N., Dean, K.P. and Watson, I. 1997. The Carboniferous of Western Europe; the development of a petroleum system. *Petroleum Geoscience*, **3**, 97–115, https://doi.org/10.1144/petgeo.3.2.97

McKirdy, D.M., Aldridge, A.K. and Ypma, P.J.M. 1983. A geochemical comparison of some crude oils from pre-Ordovician carbonate rocks. *In*: Bjorøy, M. (ed.) *Advances in Organic Geochemistry*. John Wiley and Sons, New York, 99–107.

Mews, K.S., Alhubail, M.M. and Barati, R.G. 2019. A review of brittleness index correlations for unconventional tight and ultra-tight reservoirs. *Geosciences*, **9**, 319, https://doi.org/10.3390/geosciences9070319

Moldowan, J.M., Seifert, W.K. and Gallegos, E.J. 1985. Relationship between petroleum composition and depositional environment of petroleum source rocks. *AAPG Bulletin*, **69**, 1255–1268.

Moldowan, J.M., Sundararaman, P., Salvatori, T., Alajbeg, A., Gjukic, B., Lee, C.Y. and Demaison, G.J. 1992. Source correlation and maturity assessment of selected oils and rocks from the central Adriatic Basin (Italy and Yugoslavia). *In*: Moldowan, J.M., Albrecht, J.M.P. and Philp, R.P. (eds) *Biological Markers in Sediments and Petroleum*. Prentice Hall, Englewood Cliffs, New Jersey, 370–401.

Moldowan, J.M., Peters, K.E., Carlson, R.M.K., Schoell, M. and Abuali, M. 1994. Diverse applications of petroleum biomarker maturity parameters. *Arabian Journal for Science and Engineering*, **19**, 273–298.

Morton, A., Waters, C., Fanning, M., Chisholm, I. and Brettle, M. 2015. Origin of Carboniferous sandstones fringing the northern margin of the Wales-Brabant Massif: insights from detrital zircon ages. *Geological Journal*, **50**, 553–574, https://doi.org/10.1002/gj.2572

Newport, S.M., Jerrett, R.M., Taylor, K.G., Hough, E. and Worden, R.H. 2018. Sedimentology and microfacies of a mud-rich slope succession: in the Carboniferous Bowland Basin, NW England (UK). *Journal of the Geological Society, London*, **175**, 147–262, https://doi.org/10.1144/jgs2017-036

Newport, S.M., Hennissen, J.A., Armstrong, J.P., Taylor, K.G., Newport, L.P. and Hough, E. 2020. Can One-Run-Fixed-Arrhenius kerogen analysis provide comparable organofacies results to detailed palynological analysis? A case study from a prospective Mississippian source rock reservoir (Bowland Shale, UK). *Natural Resources Research*, **29**, 2011–2031, https://doi.org/10.1007/s11053-019-09543-z

Peters, K.E. 1986. Guidelines for evaluating petroleum source rock using programmed pyrolysis. *AAPG Bulletin*, **70**, 318–329.

Peters, K.E. and Moldowan, J.M. 1991. Effects of source, thermal maturity, and biodegradation on the distribution and isomerization of homohopanes in petroleum. *Organic Geochemistry*, **17**, 47–61, https://doi.org/10.1016/0146-6380(91)90039-M

Peters, K.E., Moldowan, J.M. and Sundararaman, P. 1990. Effects of hydrous pyrolysis on biomarker thermal maturity parameters: Monterey Phosphatic and Siliceous members. *Organic Geochemistry*, **15**, 249–265, https://doi.org/10.1016/0146-6380(90)90003-I

Peters, K.E., Walters, C.C. and Moldowan, J.M. 2005. *The Biomarker Guide*. Vol. **2**, 2nd edn. Cambridge University Press, New York.

Peters, K.E., Burnham, A.K. and Walters, C.C. 2015. Petroleum generation kinetics: single versus multiple heating-ramp open-system pyrolysis. *AAPG Bulletin*, **99**, 591–616, https://doi.org/10.1306/11141414080

Quirk, M.M., Wardroper, A.M.K., Wheatley, R.E. and Maxwell, J.R. 1984. Extended hopanoids in peat environments. *Chemical Geology*, **42**, 25–43, https://doi.org/10.1016/0009-2541(84)90003-2

Riley, N.J. 1990. Stratigraphy of the Worston Shale Group (Dinantian), Craven Basin, north-west England. *Proceedings of the Yorkshire Geological Society*, **48**, 163–187, https://doi.org/10.1144/pygs.48.2.163

Rullkötter, J. and Marzi, R. 1988. Natural and artificial maturation of biological markers in a Toarcian shale from northern Germany. *Organic Geochemistry*, **13**, 639–645, https://doi.org/10.1016/0146-6380(88)90084-8

Schwark, L. and Frimmel, A. 2004. Chemostratigraphy of the Posidonia Black Shale, SW-Germany: II. Assessment of extent and persistence of photic-zone anoxia using aryl isoprenoid distributions. *Chemical Geology*, **206**, 231–248, https://doi.org/10.1016/j.chemgeo.2003.12.008

Sinninghe Damste, J.S., Kenig, F., Koopmans, M.P., Köster, J., Schouten, S., Hayes, J.M. and de Leeuw, J.W. 1995. Evidence for gammacerane as an indicator of water column stratification. *Geochimica et Cosmochimica Acta*, **59**, 1895–1900, https://doi.org/10.1016/0016-7037(95)00073-9

Słowakiewicz, M., Tucker, M.E., Vane, C.H., Harding, R., Collins, A. and Pancost, R.D. 2015. Shale-gas potential of the mid-Carboniferous Bowland-Hodder unit in the Cleveland basin (Yorkshire), central Britain. *Journal of Petroleum Geology*, **38**, 59–75, https://doi.org/10.1111/jpg.12598

ten Haven, H.L., De Leeuw, J.W., Peakman, T.M. and Maxwell, J.R. 1986. Anomalies in steroid and hopanoid maturity indices. *Geochimica et Cosmochimica Acta*, **50**, 853–855, https://doi.org/10.1016/0016-7037(86)90361-3

Timmerman, M.J. 2004. Timing, geodynamic setting and character of Permo-Carboniferous magmatism in the foreland of the Variscan Orogen, NW Europe. *Geological Society, London, Special Publications*, **223**, 41–74, https://doi.org/10.1144/GSL.SP.2004.223.01.03

Tyson, R.V. and Pearson, T.H. (eds) 1991. Modern and ancient continental shelf anoxia. *Geological Society, London, Special Publications*, **58**, https://doi.org/10.1144/GSL.SP.1991.058.01.01

Uemura, H. and Ishiwatari, R. 1995. Identification of unusual 17β (H)-moret-22(29)-ene in lake sediments. *Organic Geochemistry*, **23**, 675–680, https://doi.org/10.1016/0146-6380(95)00036-E

Volkman, J.K. 1986. A review of sterol markers for marine and terrigenous organic matter. *Organic Geochemistry*, **9**, 83–99, https://doi.org/10.1016/0146-6380(86)90089-6

Wang, C. 2007. Anomalous hopane distributions at the Permian–Triassic boundary, Meishan, China – evidence for the end-Permian marine ecosystem collapse. *Organic Geochemistry*, **38**, 52–66, https://doi.org/10.1016/j.orggeochem.2006.08.014

Wang, T.G., Simoneit, B.R.T., Philp, R.P. and Yu, C.P. 1990. Extended 8.beta.(H)-drimane and 8,14-secohopane series in a Chinese boghead coal. *Energy & Fuels*, **4**, 177–183, https://doi.org/10.1021/ef000 20a009

Waples, D.W. and Machihara, T. 1990. Application of sterane and triterpane biomarkers in petroleum exploration. *Bulletin of Canadian Petroleum Geology*, **38**, 357–380.

Waters, C.N. and Condon, D.J. 2012. Nature and timing of Late Mississippian to Mid-Pennsylvanian glacio-eustatic sea-level changes of the Pennine Basin, UK. *Journal of the Geological Society, London*, **169**, 37–51, https://doi.org/10.1144/0016-76492011-047

Waters, C.N., Waters, R.A., Barclay, W.J. and Davies, J.R. 2009. *A Lithostratigraphical Framework for the Carboniferous Successions of Southern Great Britain (Onshore)*. British Geological Survey.

Waters, C.N., Holliday, D.W. and Chisholm, J.I. 2020*a*. The contribution of publications of the Yorkshire Geological Society to the understanding of the geological development of the Carboniferous Pennine Basin, northern England. *Proceedings of the Yorkshire Geological Society*, **63**, 1–32, https://doi.org/10.1144/pygs2018-019

Waters, C.N., Vane, C.H., Kemp, S.J., Haslam, R.B., Hough, E. and Moss-Hayes, V.L. 2020*b*. Lithological and chemostratigraphic discrimination of facies within the Bowland Shale Formation within the Craven and Edale basins, UK. *Petroleum Geoscience*, **26**, 325–345, https://doi.org/10.1144/petgeo2018-039

Whitelaw, P., Uguna, C.N. *et al*. 2019. Shale gas reserve evaluation by laboratory pyrolysis and gas holding capacity consistent with field data. *Nature Communications*, **10**, 3659, https://doi.org/10.1038/s41467-019-11653-4

Yang, S. and Horsfield, B. 2020. Critical review of the uncertainty of Tmax in revealing the thermal maturity of organic matter in sedimentary rocks. *International Journal of Coal Geology*, **225**, 103–500, https://doi.org/10.1016/j.coal.2020.103500

Yang, S., Horsfield, B., Mahlstedt, N., Stephenson, M. and Könitzer, S. 2016. On the primary and secondary petroleum generating characteristics of the Bowland Shale, northern England. *Journal of the Geological Society, London*, **173**, 292–305, https://doi.org/10.1144/jgs2015-056